haematologica
Journal of the Ferrata Storti Foundation

FLI1 and GATA1 govern *TLN1* transcription: new insights into FLI1-related platelet disorders

by Elisa Gabinaud, Laurent Hannouche, Mathilde Veneziano-Broccia, Johannes Van Agthoven, Justine Suffit, Julien Maurizio, Delphine Potier, Dominique Payet-Bornet, Delphine Bastelica, Elisa Andersen, Manal Ibrahim-Kosta, Timothée Bigot, Céline Falaise, Hemostasis Unit of Lille, Anne Vincenot, Pierre-Emmanuel Morange, Paul Saultier, Marie-Christine Alessi, and Marjorie Poggi Collaborative Groups: Hemostasis Unit of Lille (Anne Bauters, Melanie Daniel, Camille Paris, Anabelle Dupont)

Received: August 1, 2024.
Accepted: December 16, 2024.

Citation: Elisa Gabinaud, Laurent Hannouche, Mathilde Veneziano-Broccia, Johannes Van Agthoven, Justine Suffit, Julien Maurizio, Delphine Potier, Dominique Payet-Bornet, Delphine Bastelica, Elisa Andersen, Manal Ibrahim-Kosta, Timothée Bigot, Céline Falaise, Hemostasis Unit of Lille, Anne Vincenot, Pierre-Emmanuel Morange, Paul Saultier, Marie-Christine Alessi, and Marjorie Poggi Collaborative Groups: Hemostasis Unit of Lille (Anne Bauters, Melanie Daniel, Camille Paris, Anabelle Dupont).
FLI1 and GATA1 govern TLN1 transcription: new insights into FLI1-related platelet disorders. Haematologica. 2025 Jan 2. doi: 10.3324/haematol.2024.286372 [Epub ahead of print]

Title

FLI1 and GATA1 govern *TLN1* transcription: new insights into FLI1-related platelet disorders

Authors

Elisa Gabinaud[1], Laurent Hannouche[1], Mathilde Veneziano-Broccia[1], Johannes Van Agthoven[2], Justine Suffit[1], Julien Maurizio[1], Delphine Potier[3], Dominique Payet-Bornet[3], Delphine Bastelica[1], Elisa Andersen[1], Manal Ibrahim-Kosta[1], Timothée Bigot[1], Céline Falaise[4], Hemostasis Unit of Lille[5], Anne Vincenot[6], Pierre-

Emmanuel Morange[1], Paul Saultier[1,4], Marie-Christine Alessi[1,4], Marjorie Poggi[1]

Collaborative Groups: Hemostasis Unit of Lille (Anne Bauters, Melanie Daniel, Camille Paris, Anabelle Dupont)

[1] Aix Marseille Univ, INSERM, INRAe, C2VN, Marseille, France

[2] Structural Biology Program, Division of Nephrology/Department of Medicine, Massachusetts General Hospital and Harvard Medical School, Charlestown, MA 02129, USA

[3] Aix Marseille Univ, CNRS, INSERM, Institut Paoli-Calmettes, CRCM, Marseille, France

[4] APHM, CHU Timone, French Reference Center on Inherited Platelet Disorders, Marseille, France

[5] Hemostasis Unit, Hospital University Center Lille, Lille, France

[6] CHU Robert Debré, National Reference Center for Inherited Platelet Disorders and Biological Hematology Service, AP-HP, Paris, France

Author contributions

EG and MP designed and performed the experiments and analyzed the data. EG, MP, and MCA analyzed the data and wrote the manuscript. MVB, JS, EA, and DB performed culture and functional experiments. LH, DP, JM, DPB, and TB performed scRNA-seq analysis. JvA conducted the structural analysis experiments. MIK, CF, PS, PEM,

Hemostasis Unit of Lille (M Daniel, C Paris, A Dupont, and A Bauters) and AV performed clinical and biological characterization of patients. MP and MCA supervised the study.

Corresponding author : Marjorie Poggi, C2VN, FSMP, 27 Boulevard Jean Moulin, 13005 Marseille, France ; e-mail : marjorie.poggi@univ-amu.fr ; Phone : +33 491 324 452.

Data-sharing statement: To obtain raw data and protocols, please contact Elisa Gabinaud (elisa.gabinaud@univ-amu.fr) or the corresponding author Marjorie Poggi (marjorie.poggi@univ-amu.fr).

Funding

The study was supported by the "Priority Research Program on Rare Diseases" of the French Investment for the Future Program (granted to MP: BIOFIT), the French Agency for Research (Agence Nationale de la Recherche - ANR, granted to MP: MOST) and by the National Institute of Health (granted to JvA : 5R01DK088327-10 and 5R01HL141366-04).

Acknowledgments

The authors acknowledge the members of the Centre de Référence des Pathologies Plaquettaires (CRPP) for their contribution regarding clinical analyses as well as the patients and healthy donors. They also thank the high-performance computing center of Aix-Marseille for granting access to its high-performance computing resources, the Génomique et Bioinformatique (GBiM) platform for the sequencing, and the Vectub platform for producing lentiviral particles.

Abstract

Germline variants of FLI1, essential for megakaryopoiesis, are linked to bleeding disorders, platelet aggregation defects and mild thrombocytopenia. However, the mechanisms behind these abnormalities remain unclear. This study aims to elucidate the impact of FLI1 variants on human megakaryocytes and platelets. We focused on four FLI1 variants, two of which are novel (p.G307R and p.R340C). We assessed the impact of FLI1 variants on megakaryopoiesis using single-cell RNA sequencing and defects were confirmed in patient platelets and cell lines. Results showed variants p.R337Q, p.K345E and p.R340C exhibited faulty nuclear localization and defective transcriptional activity *in vitro* and variants p.K345E and p.G307R affected protein stability. A total of 626 genes were differentially expressed in patient megakaryocytes, including genes associated with the platelet activation pathway. *TLN1* was among the most downregulated genes, with an 88% reduction in talin-1 protein levels in FLI1 patient platelets. Analysis of chromatin immunoprecipitation sequencing data revealed FLI1-binding regions in the *TLN1* gene. Luciferase reporter gene assays revealed the functional role of an intronic binding region in cooperation with GATA1. FLI1 variants were linked to reduced cooperative transcriptional activity. These findings reveal novel mechanisms underlying the pathogenicity of FLI1 variants. Defective cooperation between FLI1 variants and GATA1 may play a role in talin-1 deficiency in FLI1 patient platelets, thus contributing to platelet dysfunction. Moreover, talin-1 could serve as a biomarker for classifying the pathogenicity of FLI1 variants.

Main Text

Introduction

FLI1 belongs to the Ets gene family encoding transcription factors that share a conserved DNA-binding domain known as the ETS domain, which recognizes specific DNA sequences (GGA(A/T)). FLI1 plays a critical role in vasculogenesis, angiogenesis, and megakaryocytic differentiation. FLI1 can either repress or activate the expression of various megakaryocyte (MK)-specific genes by cooperating with partner transcription factors.[1–3] Mice with a targeted null *FLI1* variation die at day 11.5 of embryogenesis due to loss of vascular integrity, resulting in bleeding within the vascular plexus of the cerebral meninges.[4] Additionally, mice lacking the carboxy-terminal regulatory domain of FLI1 exhibit thrombocytopenia as well as defective platelet activation and aggregation.[5]

The role that FLI1 plays in platelet production and function in humans was initially elucidated in patients with Paris-Trousseau syndrome, who exhibit a deletion at chromosome 11q23, which includes the *FLI1* gene.[6] Germline defects in FLI1 that disrupt its transcriptional activity were documented two decades later.[7–9] These defects cause the rare constitutional bleeding disorder platelet-type 21 (BDPLT21) as listed in the Online Mendelian Inheritance in Man database. Similar to patients with an 11q23 deletion, carriers of FLI1 variants show reduced MK ploidy and size, a decrease in platelet dense granules, enlarged and fused alpha granules, and an impaired aggregation response to platelet agonists.[9] However, the effects of *FLI1* variations on FLI1 protein and megakaryopoiesis are not fully understood.

In this study, we characterized two new FLI1 variants. Transcriptome analysis of $CD34^+$-derived MKs revealed that *TLN1* is a direct target of both FLI1 and GATA1, highlighting the crucial cooperation between these two transcription factors, which is disrupted in some FLI1 variants.

Methods

The methods concerning single-cell RNA sequencing (scRNA-seq) analysis, platelet phenotyping, cell culture conditions, luciferase reporter assay, western blot assay, epifluorescence microscopy, protein stability assay, structural model of FLI1 interactions,

fibrinogen binding to platelets, electrophoretic mobility shift assay (EMSA) and proximity ligation assay are described in the *Online Supplementary Material*.

Patients and DNA sequencing

Genetic analyses were conducted at the French Reference Center for Inherited Platelet Disorders (CRPP) at La Timone University Hospital in Marseille, France. All cases were included in the study after obtaining informed written consent in accordance with protocols approved by national institutional review boards and Declaration of Helsinki principles (authorization number 20200T2-02). Four FLI1 variants were evaluated in this study, two of them p.R337Q and p.K345E (NM_002017.3, c.1009C>T and c.1033A>G, respectively) have already been reported by our team. The two additional variants p.G307R and p.R340C (NM_002017.3, c.919G>A and c.1018C>T, respectively) were discovered through sequencing of the gene panel dedicated to hereditary platelet disorders and implemented by the CRPP **.**

CD34^{+}-derived megakaryocyte culture and scRNA-seq

This was conducted as previously described.[10] After density gradient separation (Eurobio), circulating CD34^{+} cells were purified using positive selection with magnetic beads (MiltenyiBiotec) and then cultured in StemSpan Serum-Free Expansion Medium II supplemented with Megakaryocyte Expansion Supplement (STEMCELL Technologies). CD34^{+}-differentiated cells from two healthy individuals and patient A2 harboring FLI1 R337Q variant were harvested from cultures on days 5 and 11. Cell concentrations and viability were assessed after trypan blue staining with an automated cell counter (Eve^{TM} NanoEntek). The cell samples from each individual were labeled with a distinct hashtag oligo (TotalSeq-C, Biolegend) and pooled. Single-cell isolation was then carried out with the 10x Genomics Technology using the Chromium Next GEM Single Cell 5'Kit v2 (ref 1000263) according to the manufacturer's protocol. Single cell complementary DNA synthesis and sequencing libraries were prepared with a single-cell 5' Library and Gel Bead kit (10x Genomics Technology). Libraries were sequenced using a 75-bp paired-end reads format with Next-seq500 (GBiM platform) (parameters, read 1: 26 cycles, i7: 8 cycles, read 2: 57 cycles).

Statistical analyses

Quantitative variables are expressed as the mean ± standard error. Analyses were performed using GraphPad Prism software. Statistical differences were determined via Kruskal-Wallis or Mann Whitney tests as mentioned in figure legends. $P<0.05$ was considered statistically significant.

Results

Patient characteristics

Five patients were analyzed, with clinical characteristics provided in Table 1. The characteristics of affected members from families A and B have been previously documented.[9] Since the previous publication patient A2 had recurrent episodes of diffuse bilateral pulmonary hemorrhaging from 2018 to 2021, necessitating hospitalization and red blood cell (RBC) transfusions. Extensive testing did not identify a clear cause other than a platelet defect. Analysis of platelets from A1, A2, and B patients showed a defect in dense granules and reduced platelet aggregation in response to collagen, adenosine diphosphate (ADP) and thrombin receptor-activating peptide 6 (TRAP6). Patients A2 and B had mild thrombocytopenia.[9]

The proband of families C and D, ages 10 and 44, respectively, harbored novel FLI1 variants. The child of family C presented with prolonged bleeding, purpura, and epistaxis, and a bicuspid aortic valve with dilation of the ascending aorta. Platelet tests revealed reduced CD63 expression in response to TRAP6 and low mepacrine uptake, serotonin levels, and ADP consistent with a diagnostic of storage pool disease (Table S1). Electron microscopy showed large alpha granules (Figure S1). Platelet testing showed reduced aggregation responses to ADP and collagen. The 44-year-old proband from family D was assessed for moderate thrombocytopenia (86-147 $x10^9$/l) and significant bleeding episodes, including menorrhagia and postpartum hemorrhaging. Extraction of her third molars was complicated by bleeding. Surgical correction of interventricular communication required RBC transfusions. Platelet analysis revealed no platelet aggregation defects. Blood smear analysis showed giant alpha granules in several platelets (Figure S1). She exhibited decreased platelet serotonin levels and undetectable ATP release after TRAP6 stimulation, suggesting storage pool disease (Table S2).

Characterization of two novel FLI1 variants

The two newly identified FLI1 variants, G307R and R340C, were characterized and compared with the previously described variants, R337Q and K345E.[9] All mutations are located in the ETS DNA-binding domain (Figure 1A). We examined the transcriptional activity of the variants using a dual-luciferase reporter assay. Co-transfection of the reporter plasmid containing the ETS-binding sites and the plasmid encoding wild-type (WT) *FLI1* in MSR cells (GripTite293 macrophage scavenger receptor cell line) resulted in a 70% decrease in luciferase activity. Replacing WT *FLI1* with any of the *FLI1* variants, except the G307R variant, led to a significant decrease in repressive activity (Figure 1B). Western blot analysis showed that the levels of mutant FLI1 proteins exhibiting reduced activity *in vitro* were comparable to those of WT FLI1 (Figure 1C). As previously described for the R337Q and K345E variants, the biomarker MYH10 was overexpressed in the platelets of patients carrying R340C and G307R variants, while the protein was barely detected in control samples, thus confirming the pathogenicity of both novel variants (Figure 1D).

Fluorescence microscopy showed that WT FLI1 and FLI1 G307R were concentrated primarily in cell nuclei, whereas the other FLI1 variants were predominantly located in the cytoplasm (Figure 1E), thereby suggesting that the G307R variant has a distinct pathogenic mechanism. Concordant with the fluorescence microscopy results, subcellular fractionation showed increased FLI1 protein levels in the cytoplasmic fraction and decreased levels of FLI1 in the nuclear fraction in MSR cells expressing the R337Q, K345E and R340C variants compared with cells expressing WT FLI1 or the G307R variant (Figure S2).

Reduced protein stability of FLI1 variants

We assessed protein stability using cycloheximide (CHX), an inhibitor of eukaryotic translation. FLI1 protein levels were measured at different time points after CHX treatment, which is expressed as a percentage of the initial FLI1 protein levels (0 hours of CHX treatment) and normalized to GAPDH expression levels (Figure 1F). The G307R and K345E mutations led to a decrease in the half-life of the mutant proteins by approximately 60%.

Structural analysis of the FLI1-DNA interaction and FLI1 homodimers

A structural analysis shed light on the deleterious effect of each mutation. In the X-ray structure of the FLI1 DNA binding domain in complex with double stranded DNA[11] residues R337, R340 and K345 are located at the DNA/FLI1 interface (Figure 2A). Specifically, R337 and R340 form hydrogen bonds with guanine bases 5 and 4 respectively (Figure 2A, Inset A), while K345 salt-bridges the phosphate backbone (Figure 2A, Inset B). Using the SAMPDI-3D web server,[12] we calculated positive $\Delta\Delta G$ values for R337Q, R340C and K345E. While R337Q nearly reaches the critical 1 kcal/mol value (0.98 kcal/mol), R340C and K345E are clearly categorized as disruptive at 1.49 and 1.48 kcal/mol, respectively. (Table S3). In contrast, G307 is distant from the DNA/FLI1 interface and has a negligible impact on protein-DNA binding (Figure 2A and Table S3).

Additionally, we assessed the structural aspects of FLI1 homodimerization. In the FLI1 homodimer R337, R340 and K345 are away from the homodimer interface (Figure 2B). Furthermore, low $\Delta\Delta G$ values of FLI1 homodimerization upon mutations R337Q, R340C, and K345E, obtained through the Mutabind2 web server,[13] predicted a minimal effect. The G307R mutation, however, located at the core of the homodimer interface near the contact residue N306 (Figure 2B, Inset A) showed a substantial $\Delta\Delta G$ value of 3.59 kcal/mol (Table S4) potentially impeding dimerization through steric hindrance and charge repulsion.

Aberrant megakaryocyte populations in FLI1-variant cells

To investigate the impact of FLI1 variants on megakaryopoiesis, we conducted scRNA-seq on circulating $CD34^+$ cells differentiated into MKs *in vitro* and analyzed at culture days 5 and 11. The cells were derived from healthy controls and a patient carrying the R337Q mutation. We used UMAP (Uniform Manifold Approximation and Projection) dimensional reduction to visualize cell transcriptome heterogeneity. Using unsupervised clustering and lineage signature gene sets, cell types were assigned as previously described.[10] We identified the major hematopoietic cell stages: hematopoietic stem/progenitor cells (HSPCs), common myeloid progenitors (CMPs), granulocyte-monocyte progenitors (GMPs), MK-erythroid progenitors (MEPs), and progenitor and mature MKs (MKP-MKs) (Figure 3A).

In early cell stages (HSPCs, CMPs and GMPs), the transcriptome profiles of control and patient cells were highly similar. However, distinctive gene expression patterns were

observed as early as the MEP stage, which was more pronounced at the MKP/MK stage. Together with the increased FLI1 expression levels in MKs (Figure 3B), these observations indicate that FLI1 plays an important role in MK maturation. Furthermore, the number of differentially expressed genes (DEGs) between control and patient cells increased over the course of cell differentiation, especially at the MEP and MK stages (Figure S3). Erythroid-related genes are among the top 20 genes showing increased expression in patient MEPs (*HBG2*, *HBB*, *GYPB*, and *BLVRB*) and MKP/MKs (*HBE1*, *HBG2*, *HBB*, *GYPB*, *BLVRB*, and *KLF1*) (Figure S4). KLF1 was the most upregulated regulon (comprising TFs and their targets) in FLI1-deficient MK cells, and the fifth most upregulated in FLI1-deficient MEP cells (Figure S5). DEGs were enriched in various biological pathways in the KEGG gene set database (Figure 3C and Figure S6). The platelet activation pathway was the most enriched pathway for downregulated DEGs in patient MKs (Figure 3C), with 24 genes displaying decreased expression compared with control MKP-MKs (Figure 3D). Using i-cisTarget,[14] we identified ETS binding motifs significantly overrepresented in the regulatory regions of DEGs in the platelet activation pathway. The canonical FLI1 motif (M07089) had a high normalized enrichment score (NES) of 5.2. Among these 24 genes, 18 have highly ranked DNA regions for the M07089 motif, indicating they are potential direct targets of FLI1. *TLN1*, one of the most downregulated genes (fold change: 1.5, p-value<0.001), had the top-ranked FLI1-binding region (ranked first among 29 detected FLI1-binding regions) (Figure 3E).

Reduced talin-1 protein levels in FLI1 patient platelets

We confirmed the decrease in talin-1 protein levels via immunoblotting using platelet samples obtained from the five patients belonging to four different families carrying the R337Q, K345E, G307R and R340C variants, compared with age- and gender-matched healthy controls (Figure 4A). No differences were observed in other major cytoskeletal proteins, such as filamin (FlnA) or myosin heavy chain 9 (MYH9), in patient platelets compared with healthy controls (Figure S7). Additionally, we observed a decrease in fibrinogen binding by stimulated platelets derived from K345E- and R340C-variant carriers, thus indicating defective αIIbβ3 activation (Figure 4B), which cannot be attributed to a reduction in surface αIIbβ3 expression.[9]

FLI1 regulates *TLN1* transcription in cooperation with GATA1

Our findings suggest that FLI1 regulates *TLN1* expression. Silencing of endogenous FLI1 using FLI1 siRNA resulted in a decrease in talin-1 protein levels in the hematopoietic MEG-01 cell line (Figure 4C). We then acquired GATA1, RUNX1, SCL and FLI1 chromatin immunoprecipitation sequencing (ChIP-seq) data from primary human MKs (deposited by the Göttgens laboratory) from the Gene Expression Omnibus (GEO) database.[15] Peak enrichments at the *TLN1* locus were extracted and visualized using the UCSC genome browser. We identified four enriched binding regions for the FLI1 transcription factor in the *TLN1* gene (Figure 5A). One of these binding regions is situated in the *TLN1* promoter (chr9:35732119-35732518, indicated in purple). The other regions (chr9:35727623-35727967, chr9:35728277-35728673 and chr9:35729618-35730535, referred to as intronic binding sites 1, 2, and 3, respectively) are located in the first intron and also contained potential binding sites for RUNX1, SCL or GATA1.

To ascertain whether FLI1 regulates *TLN1* transcription through these binding regions we initially assessed the functionality of these binding regions using a luciferase reporter assay in HEL (human erythroleukemia) cells expressing hematopoietic transcription factors (the experimental design is described in Figure S8). Three regions (the promoter, intronic binding site 2 and intronic binding site 3) significantly increased luciferase expression, while the intronic binding site 1 region repressed luciferase expression (Figure 5B). To avoid the interference of endogenous hematopoietic transcription factors, we utilized a non-hematopoietic model, MSR cells, to identify which transcription factors bind to these regulatory regions. Based on the ChIP-seq results, we transfected transcription factors along with the putative binding sequences and evaluated luciferase activity (Figure S9). For the promoter, binding site 1 and binding site 2 sequences, the corresponding transcription factors (i.e., FLI1, FLI1 + RUNX1, and FLI1 + GATA1, respectively) were unable to regulate luciferase transcription (Figure S9). For binding site 3, we observed a significant increase in luciferase transcription activity due to co-transfection of FLI1 and GATA1 (Figure 5C). However, the simultaneous addition of SCL led to a decrease in luciferase activity, thus indicating that SCL exerts a repressive effect on the FLI1 and GATA1 cooperation. The three FLI1 variants R337Q, R340C and G307R abolished the synergistic transcriptional activation mediated by the FLI1 and GATA1 cooperation, which was not observed with the FLI1 K345E variant (Figure 5D). Co-overexpression of FLI1 and GATA1 in the MEG-01 cell line led to a significant increase in talin-1 protein levels (Figure

6A), which further supports the hypothesis that the FLI1 and GATA1 cooperation plays a role in regulating *TLN1* expression. Given the observed synergy in the transcriptional activation of *TLN1* intronic binding site 3 by FLI1 and GATA1, we performed an EMSA analysis to determine whether FLI1 and GATA1 bind to the *TLN1* intronic binding site 3 region. When *TLN1* intronic binding site 3 was incubated with nuclear proteins extracted from cells transfected with FLI1 or GATA1, specific retarded complexes were observed for both conditions. Furthermore, when *TLN1* DNA was incubated with both protein extracts, a higher molecular weight complex was formed, thus indicating that when both proteins were present, they co-bound to the DNA. Accordingly, the amount of free DNA decreased as the higher molecular weight complex formed, further reinforcing the evidence of interaction (Figure 6B). This observation corroborates our finding of several FLI1- and GATA1-binding motifs in the intronic binding site 3 sequence using the online Regulatory Sequence Analysis Tools (data not shown). We also examined the physical interaction between FLI1 (WT and variants) and GATA1 using a Duolink proximity ligation assay. The results showed that both WT FLI1 and the K345E variant interact with GATA1 in the nucleus, while the G307R, R337Q, and R340C FLI1 variants exhibited impaired interaction with GATA1 (Figure 6C).

Discussion

Pathogenic variations in the proto-oncogene *FLI1* have been linked to the dominantly or recessively inherited bleeding disorder, platelet type 21 (OMIM 617443).[7–9] In unrelated families, we discovered two novel FLI1 mutations and provided valuable phenotypic insights into this recently identified Mendelian disorder. We have previously suggested that the degree of protein dysfunction differs depending on the genetic variation.[9] Our findings suggest that various mechanisms contribute to the decrease in FLI1 activity, potentially explaining the varying levels of functional impairment. As a result, this leads to reduced expression levels of talin-1, a critical component in β3 integrin activation. The clinical symptoms observed in the carriers of the two new variants were characterized by cutaneous and mucosal bleeding. The oldest individual required RBC transfusions on several occasions. The valvular malformation in the child and history of interventricular communication in the adult patient necessitated further investigation. Both Paris

Trousseau and Jacobsen syndromes, which are caused by an 11q deletion affecting *FLI1* among numerous other genes, can involve heart malformations.[16,17] Indeed, the majority of 11q-patients have a congenital heart defect. Typically, congenital heart defects in Jacobsen syndrome are thought to be due to *ETS1* hemizygosity. *ETS1* is located close to *FLI1* and plays an important role in heart development. *ETS1*$^{-/-}$ mice display significant membranous ventricular septal heart defects at E15.5 to E17.5.[18] Several genes may be involved in the heart defect observed in patients with 11q deletion, with each gene playing a distinct role in the phenotype. As FLI1 is required to maintain endothelial cell identity, which is crucial for heart development,[19] FLI1 may also be involved in cardiac malformations. While the data from this study are not definitively conclusive, they suggest that all patients diagnosed with FLI1-related platelet disorders should undergo a cardiologic evaluation. Non-invasive diagnostic procedures, particularly cardiac and aortic ultrasounds, may detect asymptomatic cardiac defects. Early diagnosis may facilitate timely therapeutic interventions, such as the prevention of bacterial endocarditis or monitoring for aortic dilatation.

Platelet analysis of these cases suggested a diagnosis of storage pool disease, which aligns with findings from other studies.[7–9] Microscopy revealed large alpha granules in both patients. *MYH10*, which is typically suppressed during MK polyploidization,[20] was overexpressed in the patient platelets, thus indicating a defect in the repressive transcriptional activity of FLI1 *in vivo*, as previously reported.[9] Overall, the clinical profiles of both patients with the novel FLI1 variations were consistent with *FLI1* gene dysfunction. The two new variants exhibited distinct characteristics. The R340C variant exhibited a loss of repressive activity *in vitro* and cytoplasmic sequestration (similar to the previously described variants K345E and R337Q), while the G307R variant displayed normal repressive activity *in vitro* and was able to reach the nucleus. These findings suggest that the G307R variant may retain the ability to enter the nucleus and bind to DNA. The analysis of the X-ray structure of FLI1 in complex with double-stranded DNA supports this hypothesis, as the residues R340 and K345 are located at the DNA/FLI1 interface and could potentially disrupt the DNA/FLI1 interaction. By contrast, G307 is located further away from the DNA/FLI1 interface and does not affect FLI1 binding to DNA. Nuclear accumulation of FLI1 is influenced by two distinct nuclear localization signals, nuclear

localization signal 1 (at the N-terminal region, amino acids 62 to 126) and nuclear localization signal 2 (within the ETS domain, amino acids 277 to 360).[21] Mutagenesis experiments revealed the functional importance of five residues in the ETS domain of FLI1 (K325, K334, R337, R340 and K350), which may explain the nuclear import defect observed in the R337Q and R340C mutants. K345 has been shown to have a mild impact on nuclear import, thereby supporting our findings.[21] Additional mechanisms for the G307R and K345E variations were identified, potentially contributing to the observed phenotype. For example, we observed a 60% reduction in the half-life of the mutated protein. The role that homodimerization plays in the transcriptional activity of FLI1 remains unclear;[11] however, previous studies have suggested that homodimerization is significantly involved in the transcriptional activity of ETS transcription factor family members.[22,23] Analysis of the FLI1 homodimer structure revealed that R337, R340 and K345 do not participate in the homodimer interface, while G307 is located at the core of the homodimer interface and likely inhibits dimerization through steric hindrance.

Our study also aimed to identify the underlying pathological pathways for this bleeding disorder using scRNA-seq during hematopoiesis.

This study reveals an upregulation of several erythroid-related genes and the erythroid transcription factor KLF1 regulon, along with a downregulation of genes involved in megakaryopoiesis. This supports the previously described functional cross-antagonism between the transcription factors FLI1 and KLF1 in the control of erythroid versus megakaryocytic differentiation.[24–27]

This study also demonstrates the crucial role of FLI1 in the regulation of *TLN1* expression. We found that platelet activation was the most dysregulated pathway, which aligns with the previous report implicating FLI1 in the transcription of several platelet genes, including *GP6*, *GPIBA*, *GP9*, *ITGA2B*, *MPL* and *MYH10*.[7,8,28–30] More recently, transcriptome analysis of platelets harboring a DNA-binding variant of FLI1 revealed an enrichment for gene annotations related to protein transport and found that SNX24 was downregulated and required for alpha granule biogenesis.[31] In our gene expression analysis, *GP1BA* and *GP9* were among the top 20 most downregulated genes. Overall, this indicates that multiple aspects of platelet structure and function are compromised in the case of FLI1 dysfunction. We found that *TLN1* was significantly downregulated. Talin-1 is a mechano-

sensitive cytoskeleton protein that plays a central role in mechano-transduction in various tissues, such as the myocardium and blood vessels.[32] In genetic loss-of-function studies, talin-1 has been shown to be involved in the morphogenesis of heart valves.[33] Additionally, studies on zebrafish embryos carrying a *TLN1* variant have shown that a deficiency in talin-1 leads to abnormal cardiovascular morphogenesis and function, with reduced cardiac growth, ventricular shortening fraction, and heart rate.[34] Additional studies may help to determine whether FLI1 variants induce heart impairments through defective *TLN1* regulation. In platelets, talin-1 links the cytoskeleton to integrins α2β1 and αIIbβ3. Mice with selective disruption of talin-1 in MKs exhibited platelets with impaired hemostatic function and spontaneous hemorrhaging.[35] In humans, talin-1 variations have never been associated with bleeding disorders, thus suggesting that germline variations that disrupt talin-1 function may be embryonic lethal, as observed in mice.[36] By analyzing the ChIP-seq of FLI1 in MKs performed by the Göttgens laboratory,[15] four binding regions were identified in the *TLN1* gene. All binding sites were active in HEL cells. As these regions are co-occupied by FLI1, RUNX1, SCL and GATA1, we investigated potential cooperation. The FLI1-GATA1 cooperation synergistically enhanced *TLN1* transcription through binding site 3 in intron 1. This observation is consistent with earlier reports, which indicate that GATA1 binds to the FLI1 ETS domain through its zinc fingers, exhibiting significant DNA-binding cooperativity,[1] and characterized talin-1 deficiency in platelets from patients carrying a pathogenic variant of GATA1.[37] We observed a synergistic effect at the protein level in a MK-like cell line, which showed detectable levels of talin-1. Interestingly, the synergy between GATA1 and FLI1 was abolished in the case of all FLI1 mutations with the exception of the K345E mutant. The loss of synergy between GATA1 and FLI1 may provide insight into the pathogenicity of the mutated allele. The conserved synergy between K345E mutant and GATA1, despite reduced talin-1 levels in platelets from a patient carrying this variant, may be explained by the fact that the MSR model does not account for the protein instability of this variant. These findings underscore the importance of cooperation between transcription factors in the regulation of talin-1 and platelet function. Although our analysis focused on three transcription factors, other transcription factors may also be involved in *TLN1* transcription. This may explain why three of the analyzed regions lost activity in MSR cells, while activity remained in HEL cells, as MSR cells do not express most of the transcription factors involved in hematopoiesis.

In conclusion, this study describes two patients with novel FLI1 pathogenic variants, demonstrating distinct mechanisms. The study of these patients unraveled the key role of FLI1 in the regulation of *TLN1* transcription. Our findings suggest that talin-1 deficiency may contribute to the platelet dysfunction observed in patients with FLI1 variants.

References

1. Eisbacher M, Holmes ML, Newton A, et al. Protein-Protein Interaction between Fli-1 and GATA-1 Mediates Synergistic Expression of Megakaryocyte-Specific Genes through Cooperative DNA Binding. Mol Cell Biol. 2003;23(10):3427-3441.
2. Huang H, Yu M, Akie TE, et al. Differentiation-Dependent Interactions between RUNX-1 and FLI-1 during Megakaryocyte Development. Mol Cell Biol. 2009;29(15):4103-4115.
3. Bluteau D, Balduini A, Balayn N, et al. Thrombocytopenia-associated mutations in the ANKRD26 regulatory region induce MAPK hyperactivation. J Clin Invest. 2014;124(2):580-591.
4. Hart A, Melet F, Grossfeld P, et al. Fli-1 Is Required for Murine Vascular and Megakaryocytic Development and Is Hemizygously Deleted in Patients with Thrombocytopenia. Immunity. 2000;13(2):167-177.
5. Moussa O, LaRue AC, Abangan RS, et al. Thrombocytopenia in Mice Lacking the Carboxy-Terminal Regulatory Domain of the Ets Transcription Factor Fli1. Mol Cell Biol. 2010;30(21):5194-5206.
6. Breton-Gorius J, Favier R, Guichard J, et al. A new congenital dysmegakaryopoietic thrombocytopenia (Paris-Trousseau) associated with giant platelet alpha-granules and chromosome 11 deletion at 11q23 [see comments]. Blood. 1995;85(7):1805-1814.
7. Stockley J, Morgan NV, Bem D, et al. Enrichment of FLI1 and RUNX1 mutations in families with excessive bleeding and platelet dense granule secretion defects. Blood. 2013;122(25):4090-4093.
8. Stevenson WS, Rabbolini DJ, Beutler L, et al. Paris-Trousseau thrombocytopenia is phenocopied by the autosomal recessive inheritance of a DNA-binding domain mutation in FLI1. Blood. 2015;126(17):2027-2030.
9. Saultier P, Vidal L, Canault M, et al. Macrothrombocytopenia and dense granule deficiency associated with FLI1 variants: ultrastructural and pathogenic features. Haematologica. 2017;102(6):1006-1016.
10. Bigot T, Gabinaud E, Hannouche L, et al. Single-cell analysis of megakaryopoiesis in peripheral CD34+ cells: insights into ETV6-related thrombocytopenia. J Thromb Haemost. 2023;21(9):2528-2544.
11. Hou C, Tsodikov OV. Structural Basis for Dimerization and DNA Binding of Transcription Factor FLI1. Biochemistry. 2015;54(50):7365-7374.
12. Li G, Panday SK, Peng Y, Alexov E. SAMPDI-3D: predicting the effects of protein and DNA mutations on protein-DNA interactions. Bioinformatics. 2021;37(21):3760-3765.
13. Zhang N, Chen Y, Lu H, et al. MutaBind2: Predicting the Impacts of Single and Multiple Mutations on Protein-Protein Interactions. iScience. 2020;23(3):100939.
14. Herrmann C, Van de Sande B, Potier D, Aerts S. i-cisTarget: an integrative genomics method for the prediction of regulatory features and cis-regulatory modules. Nucleic Acids Res. 2012;40(15):e114.
15. Tijssen MR, Cvejic A, Joshi A, et al. Genome-wide analysis of simultaneous GATA1/2, RUNX1, FLI1, and SCL binding in megakaryocytes identifies hematopoietic regulators. Dev Cell. 2011;20(5):597-609.
16. Mattina T, Perrotta CS, Grossfeld P. Jacobsen syndrome. Orphanet J Rare Dis. 2009;4(1):9.
17. Krishnamurti L, Neglia JP, Nagarajan R, et al. Paris-Trousseau syndrome platelets in a child with Jacobsen's syndrome. Am J Hematol. 2001;66(4):295-299.

18. Ye M, Coldren C, Liang X, et al. Deletion of ETS-1, a gene in the Jacobsen syndrome critical region, causes ventricular septal defects and abnormal ventricular morphology in mice. Hum Mol Genet. 2010;19(4):648-656.
19. Weinstein N, Mendoza L, Álvarez-Buylla ER. A Computational Model of the Endothelial to Mesenchymal Transition. Front Genet. 2020;11:40.
20. Lordier L, Bluteau D, Jalil A, et al. RUNX1-induced silencing of non-muscle myosin heavy chain IIB contributes to megakaryocyte polyploidization. Nat Commun. 2012;3(1):717.
21. Hu W, Philips AS, Kwok JC, Eisbacher M, Chong BH. Identification of Nuclear Import and Export Signals within Fli-1: Roles of the Nuclear Import Signals in Fli-1-Dependent Activation of Megakaryocyte-Specific Promoters. Mol Cell Biol. 2005;25(8):3087-3108.
22. Lamber EP, Vanhille L, Textor LC, et al. Regulation of the transcription factor Ets-1 by DNA-mediated homo-dimerization. EMBO J. 2008;27(14):2006-2017.
23. Cooper CDO, Newman JA, Aitkenhead H, Allerston CK, Gileadi O. Structures of the Ets Protein DNA-binding Domains of Transcription Factors Etv1, Etv4, Etv5, and Fev. J Biol Chem. 2015;290(22):13692-13709.
24. Starck J, Cohet N, Gonnet C, et al. Functional Cross-Antagonism between Transcription Factors FLI-1 and EKLF. Mol Cell Biol. 2003;23(4):1390-1402.
25. Masuya M, Moussa O, Abe T, et al. Dysregulation of granulocyte, erythrocyte, and NK cell lineages in Fli-1 gene-targeted mice. Blood. 2005;105(1):95-102.
26. Buet D, Raslova H, Geay J-F, et al. p210BCR-ABL reprograms transformed and normal human megakaryocytic progenitor cells into erythroid cells and suppresses FLI-1 transcription. Leukemia. 2007;21(5):917-925.
27. Bouilloux F, Juban G, Cohet N, et al. EKLF restricts megakaryocytic differentiation at the benefit of erythrocytic differentiation. Blood. 2008;112(3):576-584.
28. Antony-Debré I, Bluteau D, Itzykson R, et al. MYH10 protein expression in platelets as a biomarker of RUNX1 and FLI1 alterations. Blood. 2012;120(13):2719-2722.
29. Deveaux S, Filipe A, Lemarchandel V, et al. Analysis of the thrombopoietin receptor (MPL) promoter implicates GATA and Ets proteins in the coregulation of megakaryocyte-specific genes. Blood. 1996;87(11):4678-4685.
30. Kwiatkowski BA, Bastian LS, Bauer TR, et al. The ets Family Member Tel Binds to the Fli-1 Oncoprotein and Inhibits Its Transcriptional Activity. J Biol Chem. 1998;273(28):17525-17530.
31. Lacey J, Webster SJ, Heath PR, et al. Sorting nexin 24 is required for α-granule biogenesis and cargo delivery in megakaryocytes. Haematologica. 2022;107(8):1902-1913.
32. Wang Y, Huang H, Weng H, et al. Talin mechanotransduction in disease. Int J Biochem Cell Biol. 2024;166:106490.
33. Gunawan F, Gentile A, Fukuda R, et al. Focal adhesions are essential to drive zebrafish heart valve morphogenesis. J Cell Biol. 2019;218(3):1039-1054.
34. Wu Q, Zhang J, Koh W, et al. Talin1 is required for cardiac Z-disk stabilization and endothelial integrity in zebrafish. FASEB J. 2015;29(12):4989-5005.
35. Petrich BG, Marchese P, Ruggeri ZM, et al. Talin is required for integrin-mediated platelet function in hemostasis and thrombosis. J Exp Med. 2007;204(13):3103-3111.
36. Monkley SJ, Zhou XH, Kinston SJ, et al. Disruption of the talin gene arrests mouse development at the gastrulation stage. Dev Dyn. 2000;219(4):560-574.
37. White JG, Burris SM, Thomas A. Cytoskeletons of X-Linked GATA-1, G208S Macrothrombocytes Are Deficient in Talin. Blood. 2008;112(11):1829-1829.

Table 1: Clinical characteristics of patients carrying the *FLI1* variants

Case	DNA change	AA change	Gender	Age*	Clinical features
A1	c.1010G>A	p.R337Q	Male	54	Spontaneous ecchymosis
A2	c.1010G>A	p.R337Q	Male	27	Gingivorrhagia, three episodes of lung hemorrhages
B	c.1033A>G	p.K345E	Female	60	Hematomas, epistaxis, menorrhagia, RBC transfusion during delivery and epistaxis
C	c.1018C>T	p.R340C	Male	10	Ecchymosis, prolonged bleeding from cuts, epistaxis
D	c.919G>A	p.G307R	Female	44	Ecchymosis, menorrhagia, bleeding after avulsion of wisdom teeth, abortion and delivery requiring RBC transfusion

* Age (in years) at the time of the last evaluation. AA: amino acid; RBC: red blood cell.

Figure legends

Figure 1. Functional characterization of the two novel FLI1 variants.

(A) Schematic diagram of the FLI1 protein. The functional N-terminal Pointed (PNT) and C-terminal ETS (ETS) DNA-binding domains are depicted. The position of the variations in FLI1 is indicated in red (new variations described in this study) or black (previously reported variations).

(B) MSR cells were co-transfected with an empty vector, wild-type (WT) *FLI1* or *FLI1* variant constructs, including the previously reported FLI1 variants,[9] along with the Firefly luciferase reporter plasmid containing three tandem copies of the ETS-binding site upstream of the HSV TK promoter (E743tk80Luc) and the pGL4.73 Renilla luciferase control vector. The Firefly to Renilla luminescence ratios (Fluc/Rluc) were calculated to normalize for transfection efficiency and are expressed as percentage relative to the empty vector. The data represent the mean ± SEM (standard error of the mean) of 10 independent experiments; **P<0.01, ***P<0.001, ****P<0.0001 vs. WT (Kruskal-Wallis test).

(C) Representative western blot analysis of FLI1 expression in MSR cells transfected with wild-type (WT) *FLI1* or *FLI1* variant constructs. We verified FLI1 expression using an anti-HA antibody. GAPDH was used as a protein loading control. Bottom: the results of the densitometric analysis are expressed as the mean ± SEM. Three independent experiments were performed.

(D) Representative western blot analysis of MYH10 expression in washed platelets from FLI1-variant carriers. R340C was compared to two unaffected family members (father and mother) and one unrelated control. G307R was compared to two unrelated controls. GAPDH was used as a protein loading control. Right: the densitometric analysis results were normalized to GAPDH and expressed as the mean ± SEM.

(E) Representative immunofluorescence microscopy images of H9C2 cells transfected with WT *FLI1* or *FLI1* variant constructs visualized using immunofluorescence after FLI1 (anti-HA antibody), nucleus (DAPI) and ACTIN (rhodamine phalloidin) staining; scale bar, 5 µm.

(F) The effect of FLI1 variations on the half-life of FLI1 protein. MSR cells were transfected with WT *FLI1* or *FLI1* variant constructs. After 48 hours, cells were treated with cycloheximide (CHX) for the indicated times (0, 5.5 or 9 hours (h)).

Cells were lysed, and cell lysates were then subjected to western blot analysis. Right: the densitometric analysis results are expressed as the mean ± SEM. The FLI1 levels at each time point are represented relative to the initial levels at time zero. Two independent experiments were performed.

Figure 2. Structural model of FLI1 interactions

(A) Structure of FLI1 bound to double-stranded DNA (PDB: 5e8i). The diagram shows FLI1 in pale green and the double-stranded DNA in pink cartoon. FLI1 residues G307, R337, R340, and K345 are colored in orange. Nucleotides, R337, R340 (Inset A), and K345 (Inset B) are shown in sticks at the FLI1/DNA interface. Hydrogen bonds and salt bridges are depicted in black dashed lines (< 3.5Å). Oxygen atoms are in red, nitrogen in blue and phosphorus in orange.

(B) Structure of FLI1 dimer (PDB: 5e8i). The diagram shows FLI1 monomers 1 and 2 in pale green and cyan cartoon, respectively, with residues G307, R337, R340, and K345 colored in orange. Inset A shows the FLI1 1/2 dimer with residues G307 and contact residues N306, D361, and F360 in sticks. Atoms and contacts are represented as in Figure 2A.

Figure 3. Single-cell RNA sequencing of cells derived from the FLI1 R337Q variant carrier and healthy controls

(A) UMAP plot of the FLI1 R337Q variant and control cells colored according to identified hematopoietic cell types (HSPCs, CMPs, MK-primed CMPs, GMPs, MEPs, and MKP/MKs).

(B) Violin plots showing FLI1 mRNA levels in different hematopoietic cell types from healthy subjects (left) and FLI1 patient (right). Each cell type is color-coded.

(C) Bubble plot depicting the top downregulated enriched KEGG biological pathways based on DEGs by cell type (classified by p-value). Dot sizes reflect the ratio of genes enriched in this pathway to the total number of genes in the pathway. Bubbles are color-coded according to cell type (HSPCs, CMPs, MK-primed CMPs, GMPs, MEPs, MKP/MKs).

(D) Bar plot illustrating the fold change of DEGs in the platelet activation pathway, specifically of the MKP-MK cell type.

(E) I-cis target results on the 24 genes of the platelet activation pathway. PWM: position weight matrix; NES: normalized enrichment score.

Figure 4. Talin-1 levels and fibrinogen binding in FLI1-deficient cells

(A) Western blot analysis of talin-1 expression in washed platelets from controls and FLI1-variant carriers. GAPDH was used as a protein loading control. Each patient was compared with age- and sex-matched control subjects. For each patient and matched controls, blood samples were collected at the same time and processed in parallel to avoid any bias. Quantification of band intensity is shown at the right. ***P<0.001 (Mann-Whitney test).

(B) Binding of labeled fibrinogen (Fibrinogen-FITC) to washed platelets from controls and FLI1-variant carriers (K345E ■ and R340C▲) upon activation with 10 µM TRAP6 for 15 minutes. The fibrinogen binding fold change values represent the mean fluorescent intensity (MFI) of fibrinogen bound by stimulated platelets, subtracted from the MFI under resting conditions.

(C) FLI1 siRNA were transfected into MEG-01 cells. Endogenous FLI1 and talin-1 expression levels were quantified via western blot analysis (n=3 per group). GAPDH was used as a protein loading control. Right: band intensity was quantified.

Figure 5. Identification and functional analysis of FLI1 regulatory regions in the *TLN1* gene

(A) Visualization of ChIP-seq peaks in the *TLN1* gene. FLI1, SCL, RUNX1 and GATA1 binding loci in the *TLN1* promoter region (purple) and intron 1 (yellow, orange, and green) are shown. BS: binding site.

(B) Luciferase activity in HEL cells transfected with various pGL3 luciferase reporter vectors, including the empty vector (gray), the *TLN1* promoter (purple), or *TLN1* intron 1 regions (binding site 1 in yellow, binding site 2 in orange, and binding site 3 in green). The dual-luciferase assay involved sequential measurement of Firefly and Renilla luciferase activity in the same sample; the results are presented as the ratio of Firefly to Renilla activity (Fluc/Rluc). The pGL3 vector lacking regulatory regions (empty vector) served as a normalization control. Each plasmid was assayed in three independent transfection experiments. *p<0.05 vs. pGL3-empty (Mann-Whitney test). BS: binding site.

(C) Luciferase activity in MSR cells transfected with empty luciferase reporter vector (pGL3 empty) or luciferase vector containing the intronic binding site 3 of *TLN1*

(intronic BS3), along with the pCDNA-FLI1, pCDNA-GATA1, and pCDNA-SCL vectors as specified. The pCDNA empty vector (lacking transcription factors) served as a normalization control. Each plasmid was assayed in three to six separate transfection experiments. *p<0.05, **p<0.01, ***p < 0.001 vs. pCDNA-empty vector (Kruskal-Wallis test). ##p<0.01 (Mann-Whitney test). BS: binding site; TF: transcription factor.

(D) Luciferase activity in MSR cells transfected with intronic BS3 pGL3 luciferase reporter vector and pCDNA-GATA1 with WT FLI1 or FLI1 variants as indicated. Each plasmid was assayed in two to five separate transfection experiments. *p< 0.05 vs. WT FLI1 + GATA1 (Mann-Whitney test). BS: binding site; TF: transcription factor.

Figure 6. FLI1 and GATA1 cooperation and their interaction with *TLN1* intronic binding site 3

(A) Assessment of the impact of FLI1 and GATA1 overexpression on talin-1 protein levels. Top: western blot analysis of talin-1, FLI1 (anti-FLI1 antibody), and GATA1 (anti-GATA1 antibody), in MEG-01 lysates, either non-transduced (NT) or transduced with FLI1, GATA1 or both (14 days post-transduction). GAPDH served as the loading control. Bottom: the densitometric analysis results were normalized to GAPDH and are expressed as the mean ± SEM of three independent experiments. *p<0.05 vs. NT (Kruskal-Wallis test). NT: non-transduced.

(B) EMSA assay performed with biotin-labeled *TLN1* intronic binding site 3 DNA probes and nuclear protein extracts from MSR cells transfected with either an empty vector, FLI1, or GATA1. Conditions 2 to 4 used 400 ng of nuclear extracts from cells transfected with the empty vector, FLI1, or GATA1, respectively. Conditions 5 to 7 used 400 ng of nuclear extracts from cells transfected with FLI1, combined with increasing amounts of nuclear extracts from cells transfected with GATA1 (120, 240, and 400 ng). The wedge symbol denotes these increasing GATA1 concentrations. No shift was observed in reactions without protein extract (condition 1) or with extracts from cells transfected with the empty vector (condition 2). A shift band was detected in reactions using extracts from FLI1-transfected (condition 3) or GATA1-transfected cells (condition 4), as indicated by the arrows. In reactions with extracts from cells transfected with both FLI1 and GATA1

(conditions 5 to 7), a higher molecular weight band shift was observed. FD: FLI1/DNA complexes; GD: GATA1/DNA complexes; GFD: FLI1, GATA1, and DNA complexes.

(C) The physical interactions between WT FLI1 or FLI1 variants and GATA1 in MSR cells were assessed using a proximity ligation assay, as described in the Methods section. Protein complexes of interest were visualized as red fluorescent dots, with DAPI-stained nuclei depicted in blue; scale bar, 5 μm. Top row: Microscopy images at 40X magnification. Bottom row: Zoomed-in view of a specific area of the top row images (indicated by a white dashed square). The quantification of the mean fluorescence intensity of red dots per transfected cell nucleus is shown at the bottom. *$p<0.05$, ***$p<0.001$ (Mann-Whitney test).

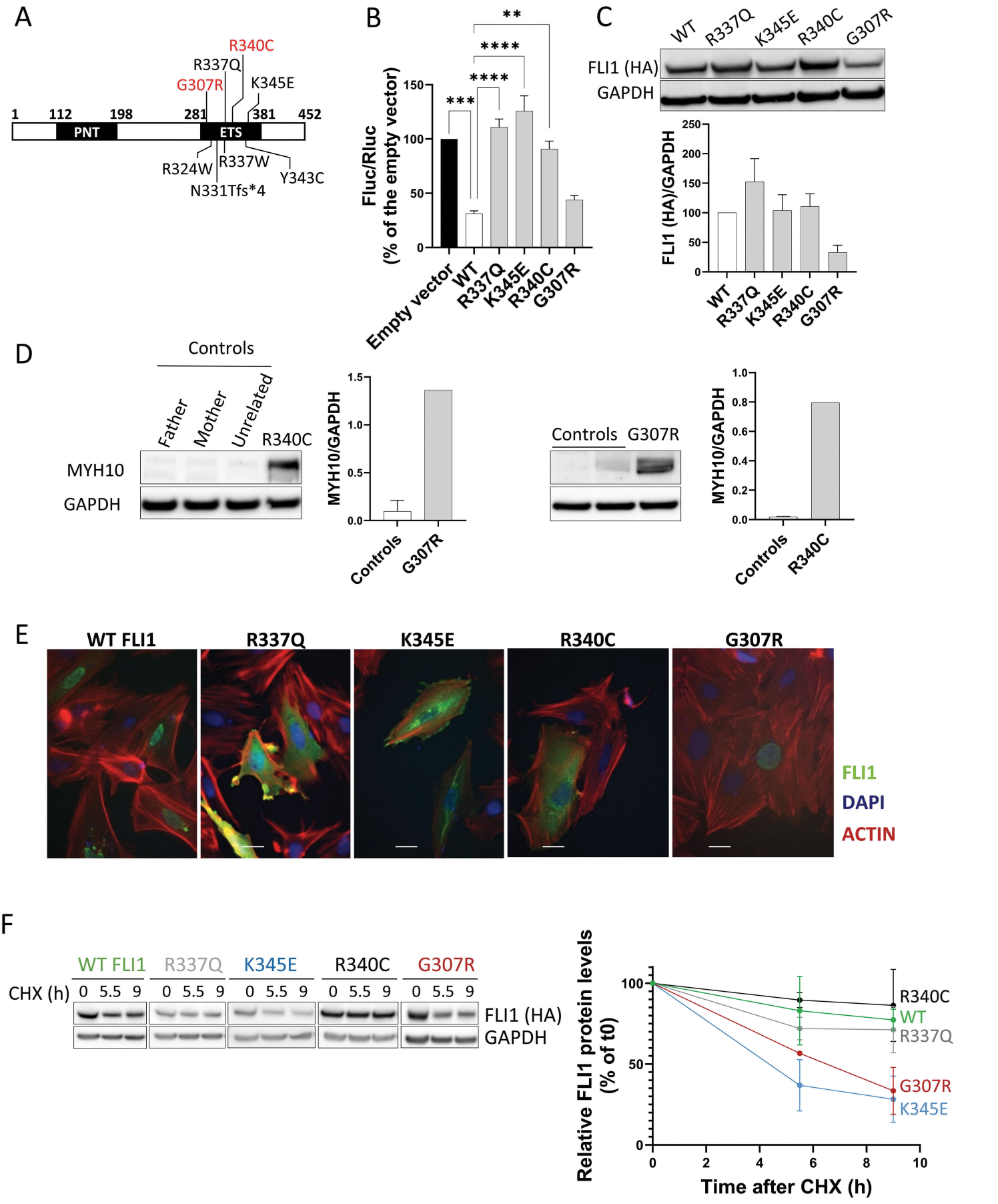
A
R340C
R337Q
G307R
K345E
1
112
198
281
381
452
PNT
ETS
R324W
R337W
Y343C
N331Tfs*4
B
Fluc/Rluc
(% of the empty vector)
150
100
50
0
***
**
****
****
Empty vector
WT
R337Q
K345E
R340C
G307R
C
WT
R337Q
K345E
R340C
G307R
FLI1 (HA)
GAPDH
FLI1 (HA)/GAPDH
250
200
150
100
50
0
WT
R337Q
K345E
R340C
G307R
D
Controls
Father
Mother
Unrelated
R340C
MYH10
GAPDH
MYH10/GAPDH
1.5
1.0
0.5
0.0
Controls
G307R
Controls
G307R
MYH10/GAPDH
1.0
0.8
0.6
0.4
0.2
0.0
Controls
R340C
E
WT FLI1
R337Q
K345E
R340C
G307R
FLI1
DAPI
ACTIN
F
WT FLI1
R337Q
K345E
R340C
G307R
CHX (h)
0
5.5
9
FLI1 (HA)
GAPDH
Relative FLI1 protein levels
(% of t0)
100
50
0
R340C
WT
R337Q
G307R
K345E
0
2
4
6
8
10
Time after CHX (h)

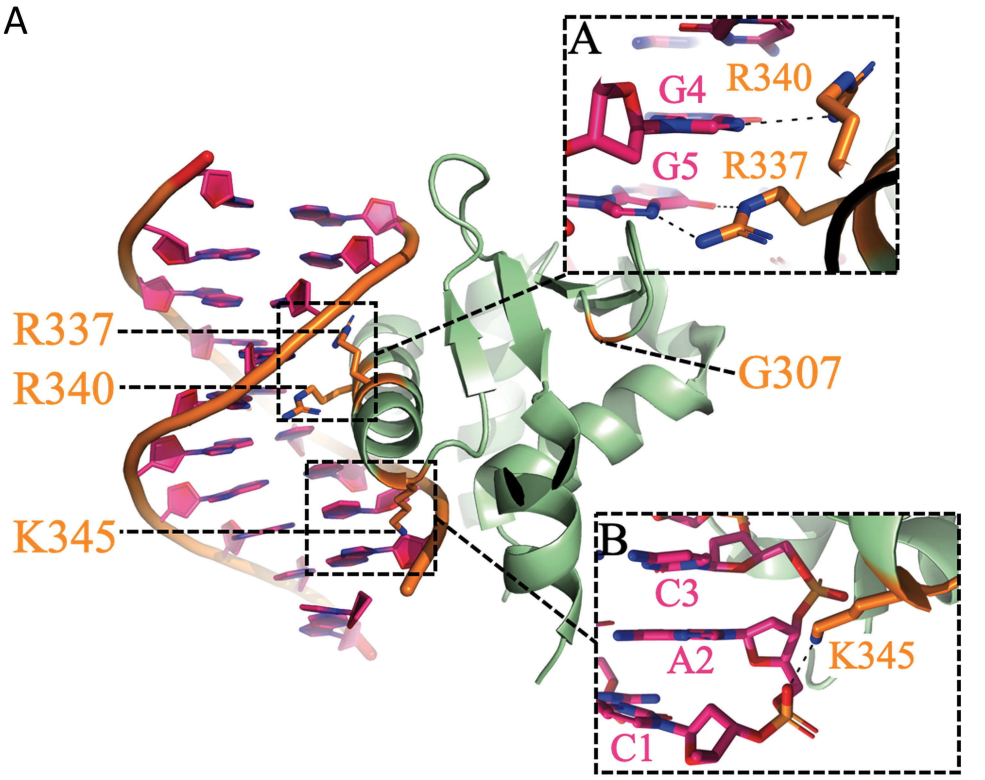
A
A
G4
R340
G5
R337
R337
R340
K345
G307
B
C3
A2
K345
C1

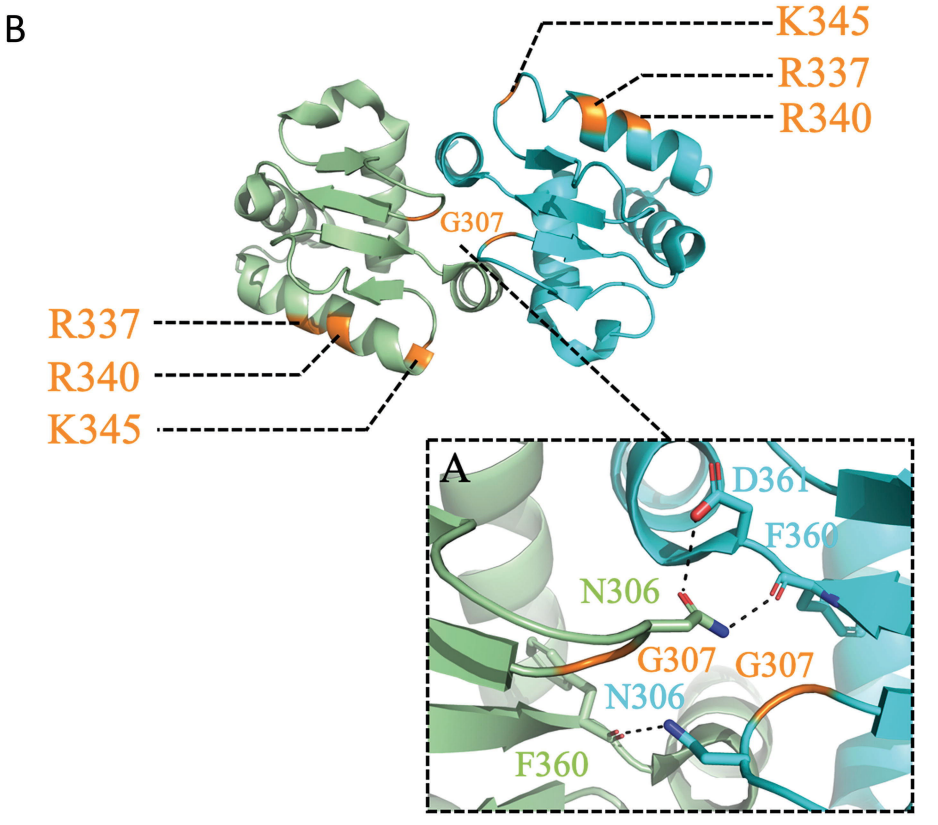
B
K345
R337
R340
G307
R337
R340
K345
A
D361
F360
N306
G307
G307
N306
F360

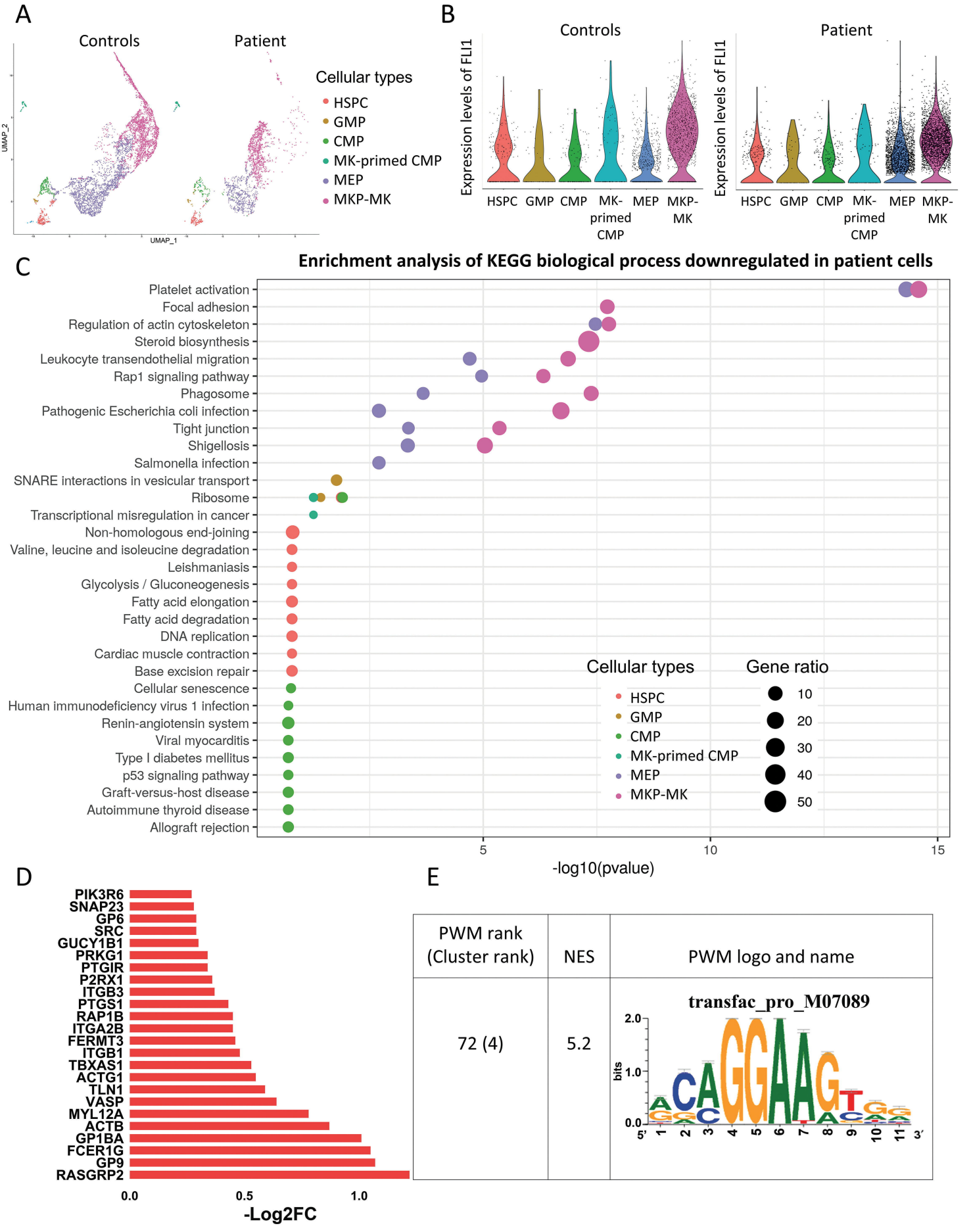
A
Controls
Patient
UMAP_2
UMAP_1
Cellular types
HSPC
GMP
CMP
MK-primed CMP
MEP
MKP-MK
B
Controls
Patient
Expression levels of FLI1
HSPC
GMP
CMP
MK-primed CMP
MEP
MKP-MK
C
Enrichment analysis of KEGG biological process downregulated in patient cells
Platelet activation
Focal adhesion
Regulation of actin cytoskeleton
Steroid biosynthesis
Leukocyte transendothelial migration
Rap1 signaling pathway
Phagosome
Pathogenic Escherichia coli infection
Tight junction
Shigellosis
Salmonella infection
SNARE interactions in vesicular transport
Ribosome
Transcriptional misregulation in cancer
Non-homologous end-joining
Valine, leucine and isoleucine degradation
Leishmaniasis
Glycolysis / Gluconeogenesis
Fatty acid elongation
Fatty acid degradation
DNA replication
Cardiac muscle contraction
Base excision repair
Cellular senescence
Human immunodeficiency virus 1 infection
Renin-angiotensin system
Viral myocarditis
Type I diabetes mellitus
p53 signaling pathway
Graft-versus-host disease
Autoimmune thyroid disease
Allograft rejection
Cellular types
HSPC
GMP
CMP
MK-primed CMP
MEP
MKP-MK
Gene ratio
10
20
30
40
50
5
10
15
-log10(pvalue)
D
PIK3R6
SNAP23
GP6
SRC
GUCY1B1
PRKG1
PTGIR
P2RX1
ITGB3
PTGS1
RAP1B
ITGA2B
FERMT3
ITGB1
TBXAS1
ACTG1
TLN1
VASP
MYL12A
ACTB
GP1BA
FCER1G
GP9
RASGRP2
0.0
0.5
1.0
-Log2FC
E
PWM rank (Cluster rank)
NES
PWM logo and name
72 (4)
5.2
transfac_pro_M07089
bits
2.0
1.0
0.0
5'
3'

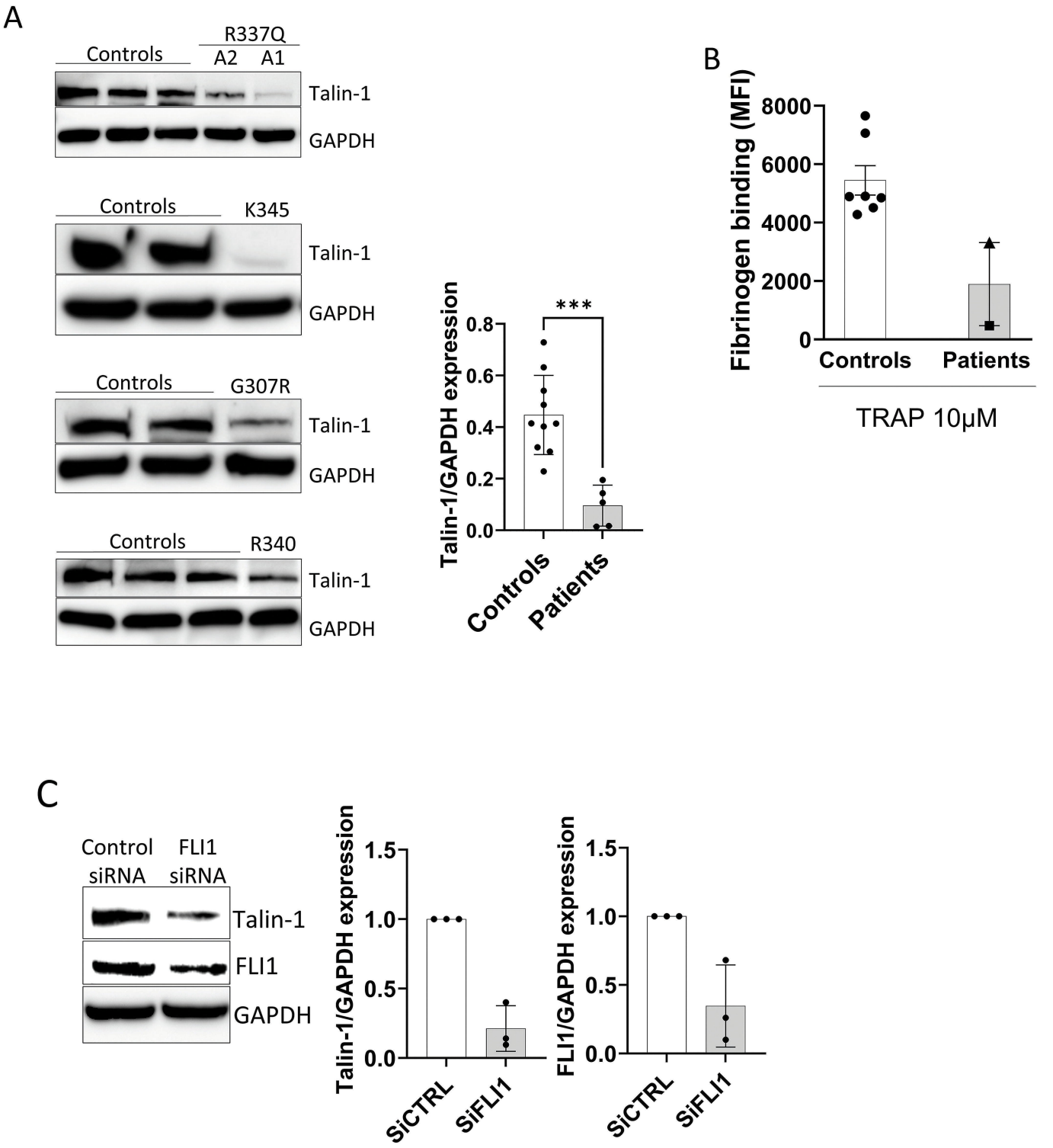
A
Controls
R337Q
A2
A1
Talin-1
GAPDH
Controls
K345
Talin-1
GAPDH
Controls
G307R
Talin-1
GAPDH
Controls
R340
Talin-1
GAPDH
Talin-1/GAPDH expression
***
0.8
0.6
0.4
0.2
0.0
Controls
Patients
B
Fibrinogen binding (MFI)
8000
6000
4000
2000
0
Controls
Patients
TRAP 10µM
C
Control siRNA
FLI1 siRNA
Talin-1
FLI1
GAPDH
Talin-1/GAPDH expression
1.5
1.0
0.5
0.0
SiCTRL
SiFLI1
FLI1/GAPDH expression
1.5
1.0
0.5
0.0
SiCTRL
SiFLI1

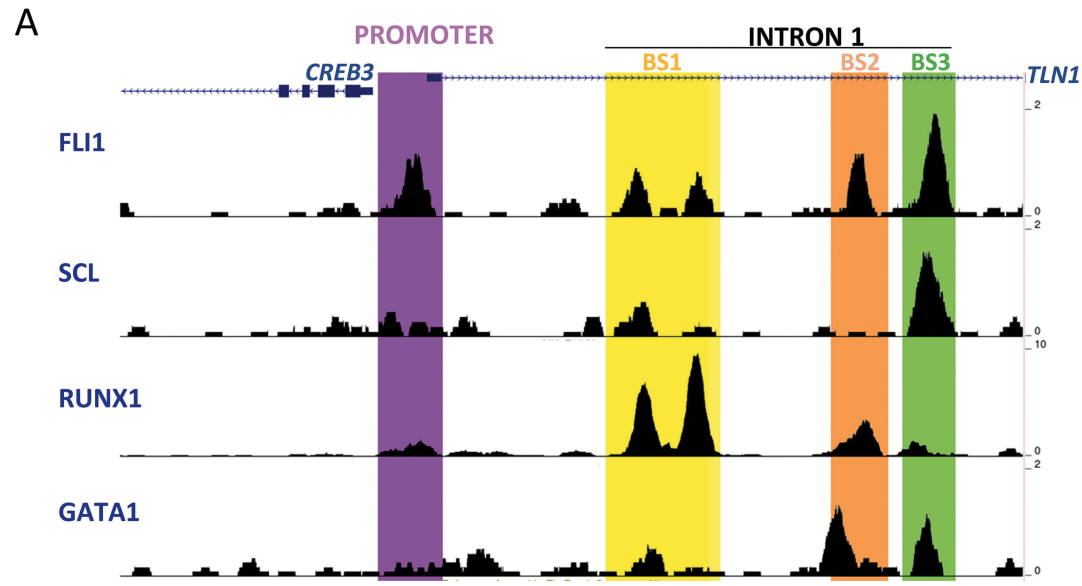
A
PROMOTER
INTRON 1
CREB3
BS1
BS2
BS3
TLN1
FLI1
SCL
RUNX1
GATA1

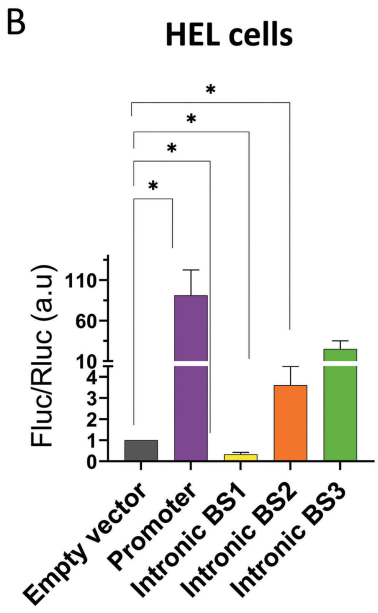
B
HEL cells
Fluc/Rluc (a.u)
Empty vector
Promoter
Intronic BS1
Intronic BS2
Intronic BS3

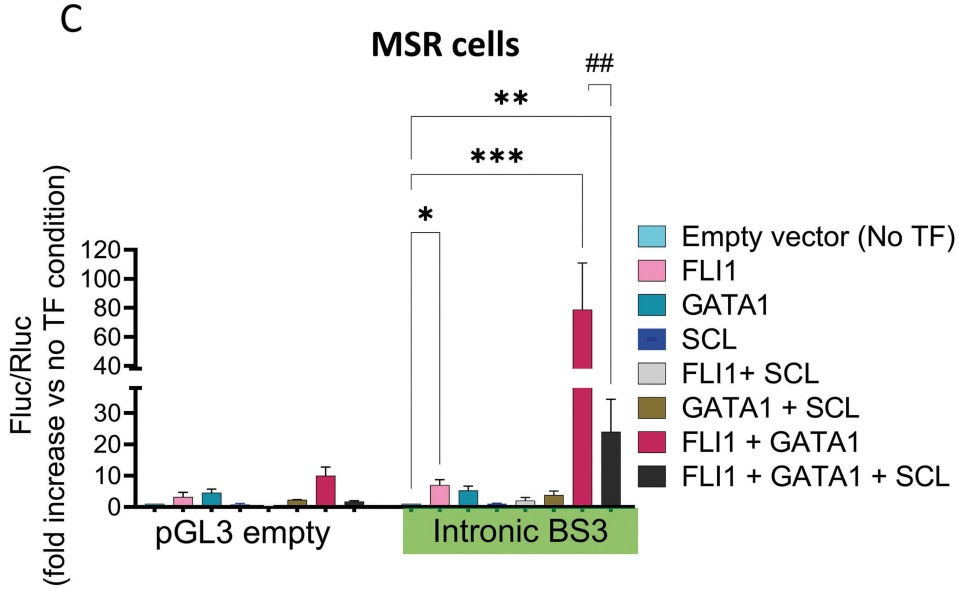
C
MSR cells
Fluc/Rluc
(fold increase vs no TF condition)
pGL3 empty
Intronic BS3
Empty vector (No TF)
FLI1
GATA1
SCL
FLI1+ SCL
GATA1 + SCL
FLI1 + GATA1
FLI1 + GATA1 + SCL

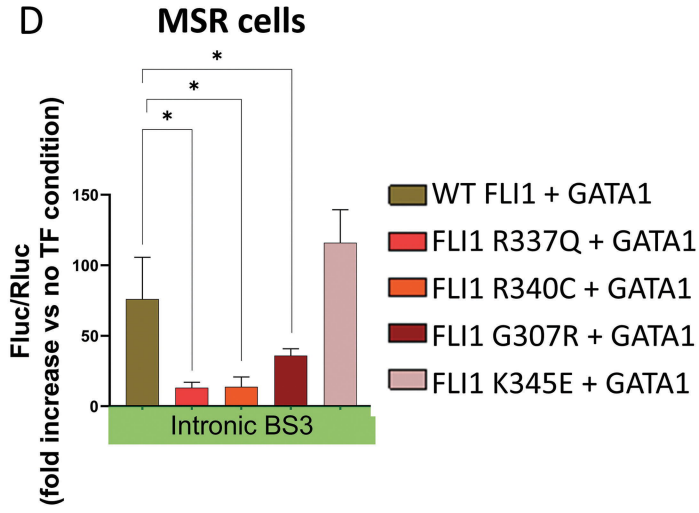
D
MSR cells
Fluc/Rluc
(fold increase vs no TF condition)
Intronic BS3
WT FLI1 + GATA1
FLI1 R337Q + GATA1
FLI1 R340C + GATA1
FLI1 G307R + GATA1
FLI1 K345E + GATA1

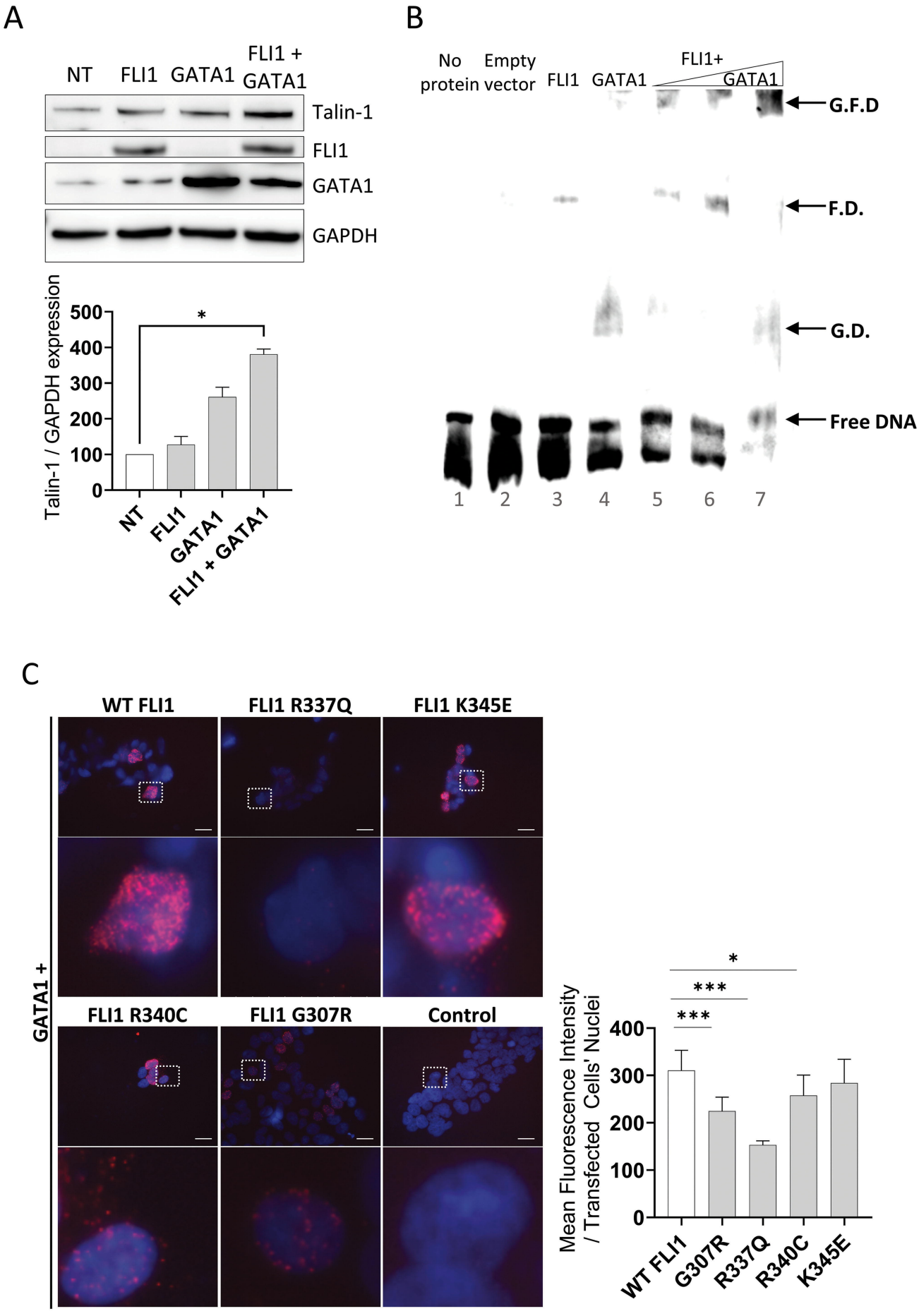
A
NT
FLI1
GATA1
FLI1 + GATA1
Talin-1
FLI1
GATA1
GAPDH
Talin-1 / GAPDH expression
500
400
300
200
100
0
*
NT
FLI1
GATA1
FLI1 + GATA1
B
No protein
Empty vector
FLI1
GATA1
FLI1+
GATA1
G.F.D
F.D.
G.D.
Free DNA
1
2
3
4
5
6
7
C
WT FLI1
FLI1 R337Q
FLI1 K345E
GATA1 +
FLI1 R340C
FLI1 G307R
Control
Mean Fluorescence Intensity / Transfected Cells' Nuclei
400
300
200
100
0
*
***
***
WT FLI1
G307R
R337Q
R340C
K345E

SUPPLEMENTARY METHODS

Analysis of single-cell RNA sequencing data

This was conducted as previously described[1]. For both scRNA-seq experiments (day 5 and day 11), mRNA library reads were aligned to the human hg38 reference genome (GRCh38-2020-A) and quantified using the cellranger count toolkit (version 5.0.0). Cell hashing antibodies were quantified using CITE-seq-Count (version 1.4.3) with default parameters. The resulting mRNA and hashtag oligo (HTO) matrices were imported into R (version 4.1.2) in order to perform downstream analyses using the Seurat package (version 4.3.0). Cells were demultiplexed using the H*TODemux and MULTISeqDemux functions except for "set5" where* HTO staining was not efficient. In addition, specific single nucleotide variants were identified for each sample using the Souporcell method (version 2.0) to rescue unassigned cells and improve demultiplexing. Associations were also confirmed between cells and samples while examining the mutation with the Integrative Genomics Viewer (IGV) and sex genes (XIST and YBX). Cell multiplets and negatives were removed from the filtered cellranger barcode matrix. Quality controls included filtering out low quality cells (i.e. cells with a feature count < 200 and with less than a 10% threshold of mitochondrial gene expression where the threshold ranged from 8 to 10% and was calculated using the scater::isOutlier function) and genes expressed in few cells (e.g., genes expressed in less than 3 cells). Samples from the two time points (days 5 and 11) were merged using the Seurat merge function. The merge quality and absence of batch effects were subsequently assessed by overlapping several cell groups at both time points. After normalization and regression scaling based on cell cycle genes, two-dimensional reduction was performed. The merged object was reduced using principal component analysis (PCA) (Seurat::RunPCA) with the 1000 most variable genes (Seurat::FindVariableFeatures). The PCA reduction was used to generate a UMAP with the first 10 components (Seurat::RunUMAP). The nearest-neighbor graph (k-nn) was generated using the Seurat::FindNeighbors function with a k parameter equal to 12 and the first 8 components merging datasets. Cell clusters were defined using the Seurat::FindClusters function with the Louvain algorithm (resolution of 0.4). This Seurat analysis was split between controls and FLI1 patient and each subset object was individually processed as previously mentioned. Based on our previously published hematopoietic gene signature[1] and the top 20 cluster differentially expressed genes, cell type-specific signatures were adapted, scored for controls and patient independently and assigned to each cluster. These assignments were transferred onto the merged object and differential gene expression analysis was performed for each cell type (controls vs. FLI1 patient) with a log fold-*change threshold equal to 0 and using the "bimod"* test (Likelihood-ratio test for single cell gene expression).[2] Differentially expressed genes with

a p-value < 0.05 and either average log2 fold change > 0 or average log2 fold change < 0 were filtered. An enrichment analysis was performed on five different databases (Transfac and Jaspar, KEGG 2019, GO Biological process 2018, Reactome 2016 and Transcription factor PPI) and summarized in bubble plots. To infer gene regulatory networks implicated in FLI1-related transcriptome dysregulation, we used the SCENIC method using a cellranger-filtered raw unique molecular identifier (UMI) matrix. All statistical tests comparing patients to controls were performed using the Wilcoxon test, with a p-value < 0.05 considered statistically significant.

Data and code availability

All the sequencing data has been deposited in NCBI*'s* Gene Expression Omnibus and are accessible through GEO series accession number (GSE273210). The human transcriptome reference used in our study is available on 10X Genomics website (https://cf.10xgenomics.com/supp/cell-exp/refdata-gex-GRCh38-2020-A.tar.gz) or Zenodo (https://zenodo.org/uploads/12759766). Docker images and detailed scripts used for preprocessing and further analysis are available at Zenodo (https://zenodo.org/uploads/12759766) and GitHub (https://github.com/poggiteam/FLI1_2021), respectively.

Light transmission platelet aggregation

Citrated blood was collected by antecubital venipuncture into Becton-Dickinson vacutainer tubes containing 0.105 mol/L trisodium citrate. Platelet-rich plasma (PRP) was prepared in accordance with the ISTH recommendations.[3,4] Platelet aggregation was assessed by measuring light transmission through the stirred suspensions of PRP for 5 min using an APACT 4004 aggregometer. Platelet aggregation was triggered by adding 2.5 and 5 µM adenosine diphosphate (ADP; Helena Laboratories) and 2 µg/ml collagen (Bio/Data Corporation).

Evaluation of platelet granules

Electron microscopy was performed as previously described.[5] For the intraplatelet serotonin measurement, the PRP was subjected to two freeze/thaw cycles. An automated platelet count of the PRP was performed prior to the serotonin measurement in order to normalize the serotonin level to the platelet count; results were expressed as µg/10^9 platelets. The plasma serotonin level was considered negligible as compared to the intraplatelet serotonin content. Serotonin was quantified using high-performance liquid chromatography (HPLC) (Dionex,

Thermo Scientific©) coupled with electrochemical detection (Precision Instruments©, Model 105).

Platelet ATP/ADP levels were assessed using HPLC on an anion exchange column. Assays have been performed at the Hemostasis Laboratory-EFS-Strasbourg-France.

The Mepacrine test was performed as previously described.[5] Briefly, PRP count was adjusted to 10 platelets x 10^9/L. Platelet mepacrine uptake was assessed after 30 minutes incubation at 37°C without or with mepacrine (Quinacrine dihydrochloride, Cas number 69-05-6, Sigma) at 1 and 2 µmol/L final concentration.

MSR cell culture

GripTite™ 293 cells (a genetically engineered Human Embryonic Kidney (HEK 293) cell line that expresses the human macrophage scavenger receptor, Thermo Fisher Scientific) were cultured in DMEM supplemented with 10% fetal bovine serum, 100 U/mL penicillin, 0.1 mg/mL streptomycin, 1% GlutaMAX™ and 1% non-essential amino acids.

Luciferase reporter assay

Transcriptional regulatory properties of WT FLI1 and FLI1 variants were analyzed using the E743tk80Luc plasmid containing the luciferase gene driven by an enhancer cassette comprised of three tandem copies of the Ets *Binding Site (EBS) inserted 5' of the herpes* simplex virus thymidine kinase promoter, as previously described[6]. Directed mutagenesis of the human expression plasmid pCMV3-FLI1-HA (Sino Biological Inc.) was performed using the GeneArt Site-directed Mutagenesis System kit (Thermo Fischer Scientific) according to the *manufacturer's instructions.* GripTite™ 293 MSR Cells, a genetically engineered Human Embryonic Kidney 293 cell line (Thermo Fisher Scientific), were transfected using PolyJet In Vitro DNA Transfection Reagent (SignaGen Laboratories). The transfection included the reporter gene constructs (150 ng), the expression plasmid (330 ng) and SV40-driven luciferase plasmid (pGL473-hRLuc) (10 ng) for normalization of transfection efficiency.

The identified regulatory regions in the *TLN1* gene were cloned into a pGL3 vector and confirmed using Sanger DNA sequencing (Proteogenix). To investigate cell-type dependence, the HEL (human erythroleukemia) hematopoietic and GripTite 293 MSR cell lines were used. Transfections with expression plasmids (*FLI1*, *GATA1*, *RUNX1,* and *SCL*) and the pGL3 vector along with the pGL473-hRLuc for normalization, were carried out using PolyJet In Vitro DNA Transfection Reagent. The cells were harvested and lysed 48 hours post-transfection and Firefly and Renilla luciferase activities were measured consecutively using the reporter gene

detection kit (Yelen) with an EnSight™ Multimode Microplate Reader (PerkinElmer) according *to the manufacturer's instructions.*

Western blot assay

To isolate nuclear and cytoplasmic subcellular fractions from protein lysates, MSR cells were lysed 48h after transfection (PolyJet In Vitro DNA Transfection Reagent, SignaGen Laboratories). Fractionation was performed using the NE-PER Nuclear and Cytoplasmic Extraction Reagent (Pierce). Total platelet proteins from washed platelets and proteins from the subcellular fractions were separated on NuPAGE gels with MES SDS running buffer (Thermo Fisher Scientific) and transferred onto a polyvinylidene fluoride membrane. Membranes were blocked and labeled overnight with the following primary antibodies: rabbit anti-FLI1 (Santa Cruz Biotechnology; ref: sc-356), rabbit anti-HA (Santa-Cruz Biotechnology; sc-805), rabbit anti-MYH10 (Santa Cruz Biotechnology; sc-376942), rabbit anti-LAMIN-B1 (sc-374015), mouse anti-Talin (sc-365875), rabbit anti-MYH9 (Protein tech; 11128-1-AP), mouse anti-FlnA (Santa Cruz Biotechnology; sc17749), and mouse anti-GAPDH (Millipore; MAB374). Horseradish peroxidase–conjugated secondary antibodies (Bio-Rad) were used, and chemiluminescence signals were obtained using Pierce ECL Western Blotting Substrate (Thermo Fisher Scientific; 32106) or Ultra High Sensitivity ECL kit substrate (MedChem Express; HY-K1005). Images were captured using a CCD Imager ImageQuant LAS 4000 (GE Healthcare) and quantified using ImageJ software (National Institutes of Health, Bethesda, Maryland).

H9C2 cell culture

H9C2 cells (cell line derived from embryonic BD1X rat heart tissue; ATCC CRL-1446) were cultured in DMEM supplemented with 10% fetal bovine serum, 100 U/mL penicillin, 0.1 mg/mL streptomycin, and 1% GlutaMAX™.

Epifluorescence microscopy

MSR cells or H9C2 cells were fixed in 1% paraformaldehyde for 15 minutes at room temperature 48 hours after transfection. After washing, cells were permeabilized with 0.3% Triton X-100 in PBS for 10 minutes, blocked for 30 minutes using 1% BSA-PBS and incubated overnight with rabbit anti-HA antibody (Santa Cruz Biotechnology; sc-805). Subsequently, cells were incubated with anti-rabbit Alexa 488-labeled secondary antibody (Abcam; ab150077) and then with phalloidin rhodamine (Cytoskeleton, Inc. PHDR1) for 30 minutes. After washing

steps, slides were mounted with DAPI-Fluoromount for examination using an AXIO Imager M1 microscope (Carl Zeiss, Germany).

Protein stability assay

GripTite™ 293 MSR cells were transfected with pCMV3-FLI1-HA (WT and FLI1 variants). After 48 hours cells were treated with 50 *μ*g/mL cycloheximide (CHX) (Sigma; C-6255) to inhibit protein synthesis. Cells were harvested at different time points (0, 5.5, and 9 hours) and processed for immunoblotting with anti-HA and anti-GAPDH antibodies.

Structural model of FLI1 interactions

Prediction of affinity changes. The impact of mutations on the FLI1-DNA interaction was analyzed through *ΔΔ*G predictions on the structure of FLI1 in complex with a 10-mer of double-stranded DNA ACCGGAAGTG (PDB code 5e81) using the protein-DNA SAMPDI-3D Web server (compbio.clemson.edu/ SAMPDI-3D/#started). SAMPDI-3D applies *ΔΔ*G values derived from physico-chemical and structural properties of the mutated protein-DNA site to a gradient lifting machine learning algorithm based on a large, high-quality dataset.[7] MutaBind2 *was utilized to assess changes in binding affinity (ΔΔG) caused by FLI1 mutations (G307R,* R337Q, R340C, and K345E) on the FLI1 homodimer within the FLI1/DNA structure (PDB code 5e8*). MutaBind2 calculates ΔΔG values* based on side-chain optimization and multiple rounds of energy minimization algorithms incorporating molecular mechanics and static force fields.[8]

Fibrinogen binding to platelets

One hundred microliters of RPMI-diluted platelets at a concentration of 6 x10^3 platelets/µL were incubated with 10 µL of a rabbit anti-fibrinogen conjugated to FITC (Thermo Fisher Scientific RB-1924-R2) and 90 µL of PBS, with or without TRAP6 (10 µM), for 15 minutes at room temperature. Fibrinogen binding was measured using flow cytometry. Results are expressed as mean fluorescence intensity.

MEG01 cell culture

MEG01 cells were obtained from Sigma and cultured in RPMI-1640 supplemented with 10% fetal bovine serum, 100 U/mL penicillin, 0.1 mg/mL streptomycin, and 1% GlutaMAX™.
For siRNA treatments, 250,000 cells underwent 2 sequential transfections with 10 pmol of control siRNA (Santa Cruz; 37007) or 10 pmol of FLI1 siRNA (Santa Cruz; 35384).

Transfections were performed on days 1 and 4 using the PepMute™ Plus siRNA Transfection Reagent (SignaGen Laboratories; SL10057). Cells were lysed with RIPA on day 7.
For transduction, *GATA1* and *FLI1* DNA were subcloned into a lentiviral vector pRRLSIN-MND-IRES2-ZsGreen-WPRE, and lentiviral particles were prepared by VectUb platform at Bordeaux University. MEG01 cells were transduced with a multiplicity of infection (MOI) of 7.5, to overexpress FLI1 and with a MOI of 25 to overexpress GATA1, then lysed with RIPA after 2 weeks.

Electrophoretic mobility shift assay

Nuclear extracts were prepared from MSR cells transfected with either the empty vector, WT *FLI1,* or *GATA1,* using the Pierce NE-PER Nuclear and Cytoplasmic Extraction Kit, according to the manufacturer's instructions. *Cell extracts were stored at −80°C until use.* The oligonucleotides used in EMSA analysis were synthesized and labeled with streptavidin by Proteogenic as follows: intronic BS3 of *TLN1, 5'*-TAT CCG CTT GTG TCC CAG CTG GAC AGA CCT GGC TAT GGG GTT GCT GAC CAT GAA AGA ATG AGG GCT GGG CTG GTG GAT CCG AGA AGC TGG AGG AGT CTG TGG AGC CAA GAA GCA GGA CTG AAA GGA CCC TTC ACA CTA AGC TGA AAC TGC ATG TCT CCC CCC ATT TCC TCT GGA CAC TTA GAC ACC CCC TTC CTC CTC AAG CAC GGA AGC CTC TGG TGA GAC CCC GAT AAG GGA GCT GAG TCA TGC CTA CCC TTA CTC CCC AGC TGG TCC AGA GTG GAT ATT CAC ACA GCT ACA AGA GGG TGT GTG GAC GCG AAG AAC TGA TCA GTG AAT TGT GGG T-*3'. The labeled oligonucleotides were then incubated with* nuclear extracts in the binding buffer (from Light Shift kit, Thermo Fisher Scientific 20148X). Binding reactions were performed in 20 µl containing 1 fmol oligonucleotides, 1X binding buffer, 1µg of poly (dI-dC), 50% glycerol, 1% NP40, 100 mM MgCl2, 1X charge buffer (Thermo Fisher Scientific, 20148X). The samples were then run on a native 6% polyacrylamide gel. The contents of the gel were then transferred to a nylon membrane (Thermo Fisher Scientific, 77015) and crosslinked to the membrane using a UV crosslinker. Membranes were blocked and then visualized using the reagents provided in the Light Shift kit.

Protein interaction studies

Detection of FLI1 and GATA1 interaction in MSR cells was performed using the Duolink® In situ Detection Reagents (Sigma-*Aldrich, St. Louis, MO, USA) according to the manufacturer's* instructions. Briefly, MSR cells were first incubated with two primary antibodies that recognize the target proteins, rabbit anti-HA (Thermo Fisher Scientific, 71-5500) and mouse anti-c-MYC (Santa Cruz, sc-40) antibodies, and then incubated with a pair of proximity ligation assay (PLA)

probes consisting of species-specific secondary antibodies (anti-rabbit and anti-mouse) conjugated to complementary oligonucleotides. In the presence of hybridization solution and ligase, the oligonucleotides form a circle when the proteins are in close proximity. Finally, the polymerase and nucleotides participate in the formation of rolling circle amplification, which is visualized as red fluorescence. After washing steps, slides were mounted with DAPI-Fluoromount for examination using an AXIO Imager M1 microscope (Carl Zeiss, Germany).

REFERENCES

1. Bigot T, Gabinaud E, Hannouche L, et al. Single-cell analysis of megakaryopoiesis in peripheral CD34+ cells: insights into ETV6-related thrombocytopenia. *J Thromb Haemost*. 2023;S1538-7836(23)00321–5.
2. McDavid A, Finak G, Chattopadyay PK, et al. Data exploration, quality control and testing in single-cell qPCR-based gene expression experiments. *Bioinformatics*. 2013;29(4):461–467.
3. Cattaneo M, Cerletti C, Harrison P, et al. Recommendations for the standardization of light transmission aggregometry: a consensus of the working party from the platelet physiology subcommittee of SSC/ISTH. *J Thromb Haemost*. 2013;11(6):1183–1189.
4. Gresele P, Subcommittee on Platelet Physiology of the International Society on Thrombosis and Hemostasis. Diagnosis of inherited platelet function disorders: guidance from the SSC of the ISTH. *J Thromb Haemost*. 2015;13(2):314–322.
5. Saultier P, Vidal L, Canault M, et al. Macrothrombocytopenia and dense granule deficiency associated with FLI1 variants: ultrastructural and pathogenic features. *Haematologica*. 2017;102(6):1006–1016.
6. Poggi M, Canault M, Favier M, et al. Germline variants in ETV6 underlie reduced platelet formation, platelet dysfunction and increased levels of circulating CD34+ progenitors. *Haematologica*. 2017;102(2):282–294.
7. Li G, Panday SK, Peng Y, Alexov E. SAMPDI-3D: predicting the effects of protein and DNA mutations on protein–DNA interactions. *Bioinformatics*. 2021;37(21):3760–3765.
8. Zhang N, Chen Y, Lu H, et al. MutaBind2: Predicting the Impacts of Single and Multiple Mutations on Protein-Protein Interactions. *iScience*. 2020;23(3):100939.

SUPPLEMENTARY FIGURES

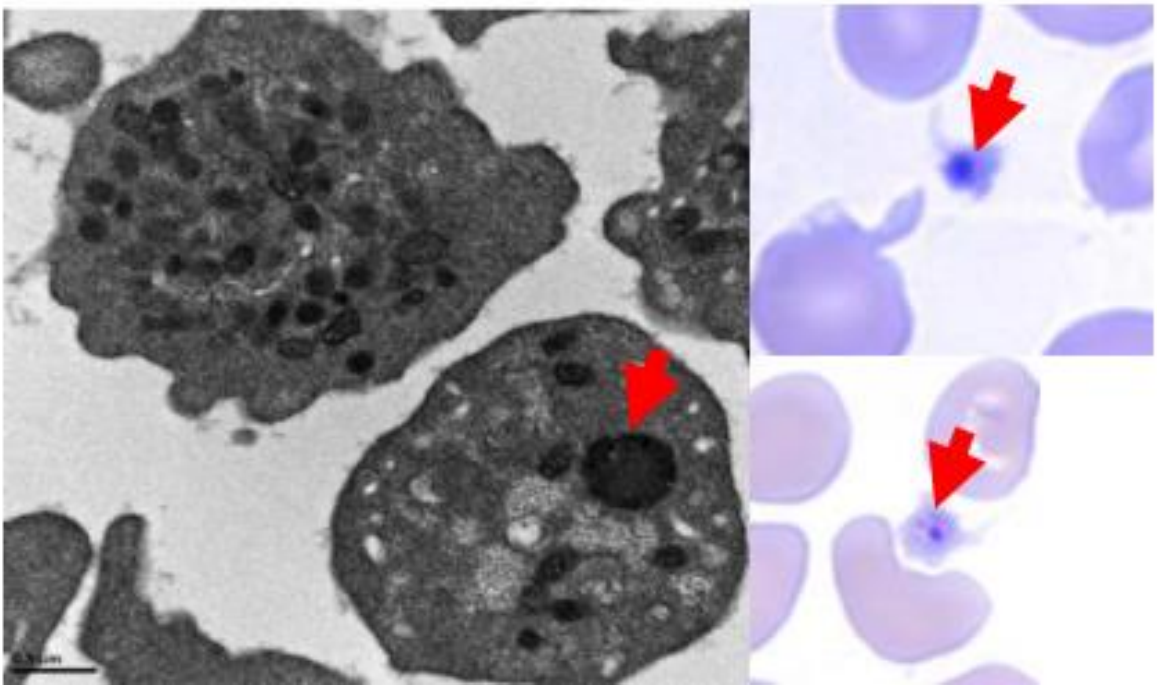

Figure S1: **Giant alpha granules in patient platelets.** Left: Electron microscopy image of platelets from the patient carrying the R340C variant; scale bar, 0.5 µm. Right: Blood smears showing platelets from the patient with the G307R variant. Red arrows indicate giant alpha granules.

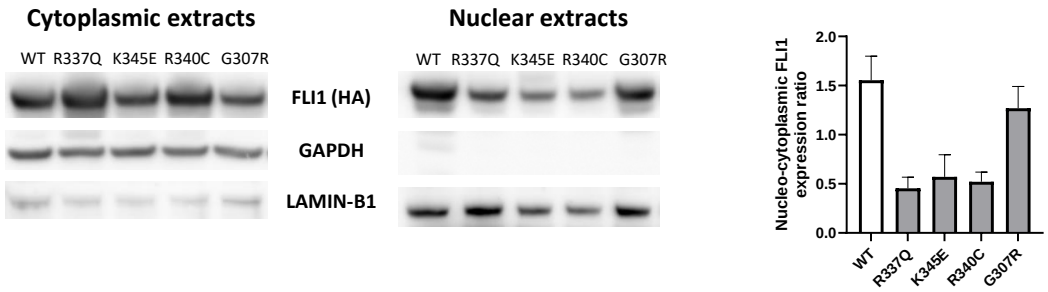

Figure S2: Western blot analysis of WT FLI1 and FLI1 variant subcellular localization. MSR cells were transfected with WT *FLI1* or *FLI1* variant constructs. LAMIN-B1 and GAPDH expression levels were used as nuclear and cytoplasmic markers, respectively. Data are represented as the mean ± SEM of two independent experiments.

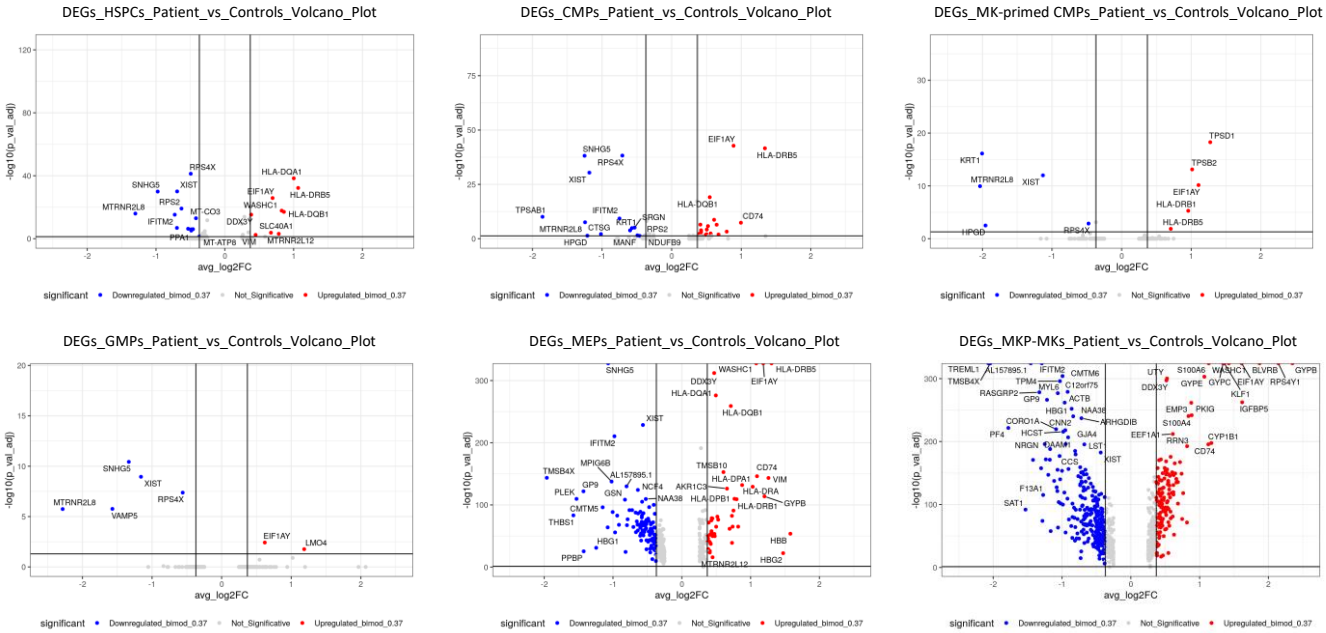

Figure S3: Differentially expressed genes between patient and controls during MK cell differentiation. Volcano plots depicting log2 fold change and false discovery rate–adjusted p-values. The panels compare gene expression levels between patient and controls at various cellular stages (HSPCs, CMPs, MK-primed CMPs, GMPs, MEPs, and MKP-MKs). Differentially expressed genes (DEGs) with a fold change >1.3 or < -1.3 and a P<0.05 are shown in red or blue, respectively.

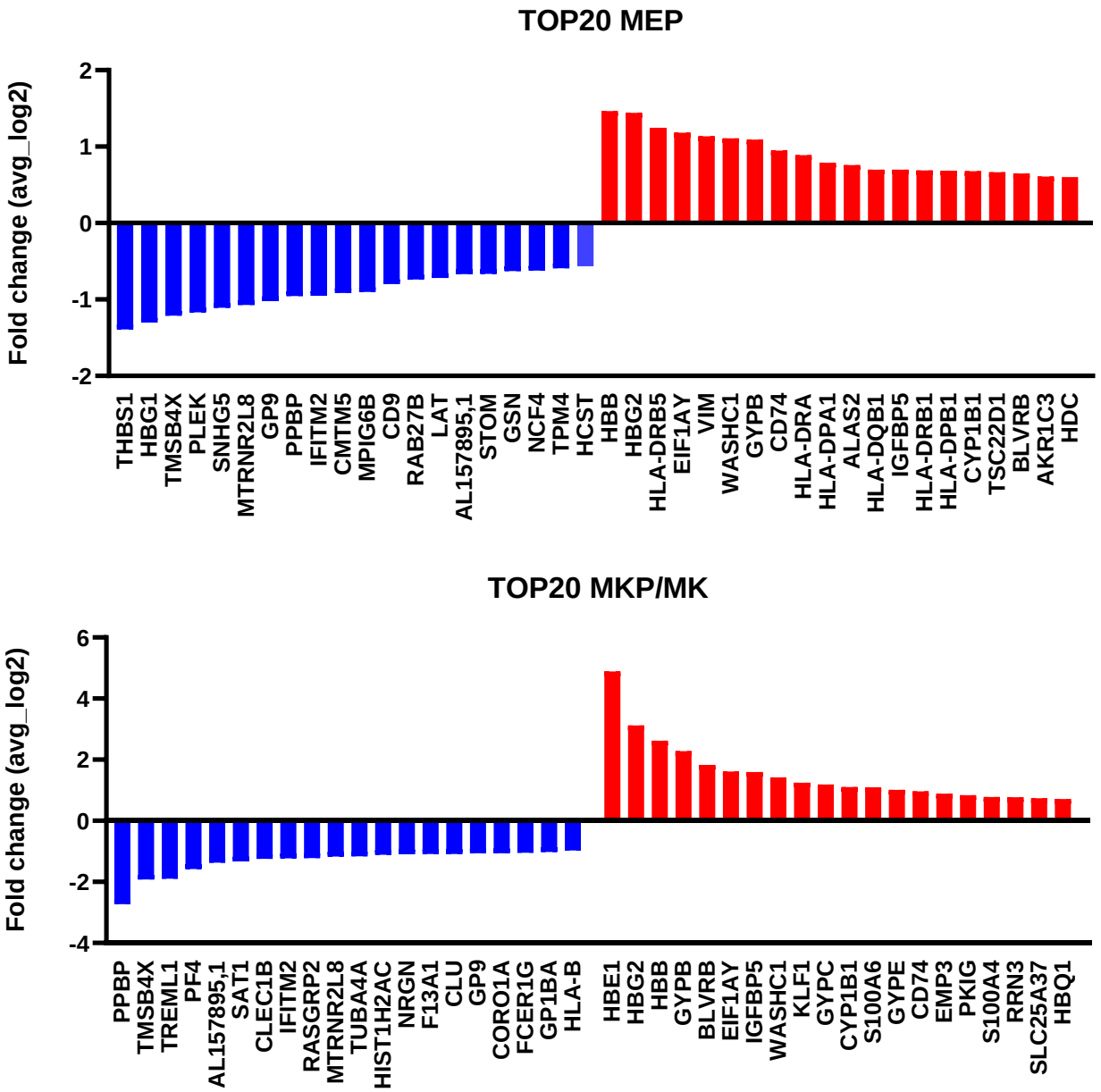

Figure S4: The top 20 differentially expressed genes in patient MEPs and MKP/MKs. Downregulated (depicted in blue) and upregulated genes (depicted in red) in FLI1-mutated MEP and MKP-MK cells compared with control cells ($p<0.05$) and classified according to log2 fold change.

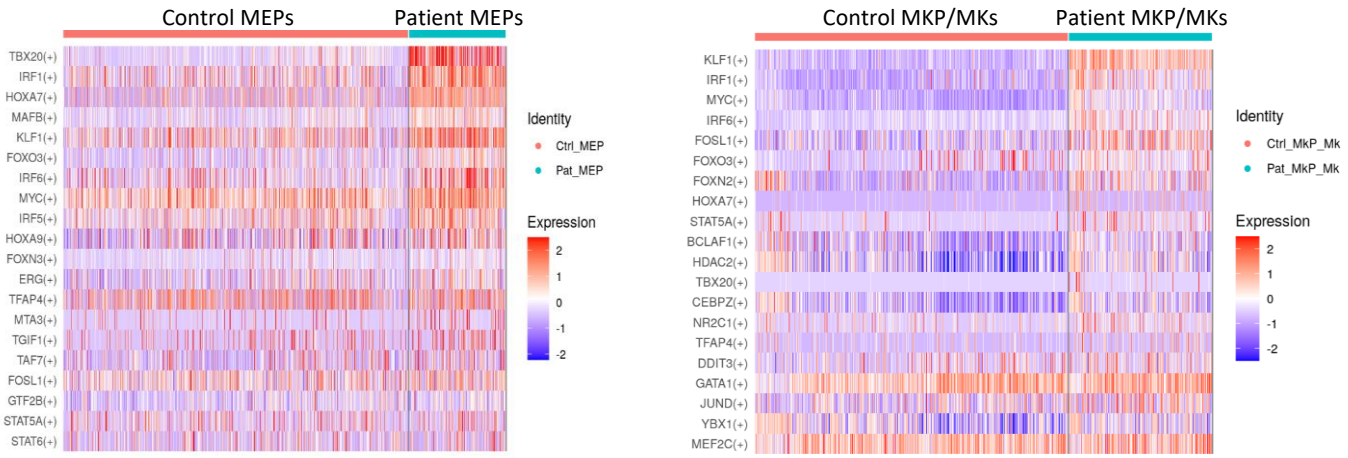

Figure S5: Heatmap showing the top 20 differentially active regulons (patient vs controls). Differentially active regulons in MEPs are displayed on the left, while those for MKP/MKs are shown on the right. The color gradient corresponds to the scaled regulon activity.

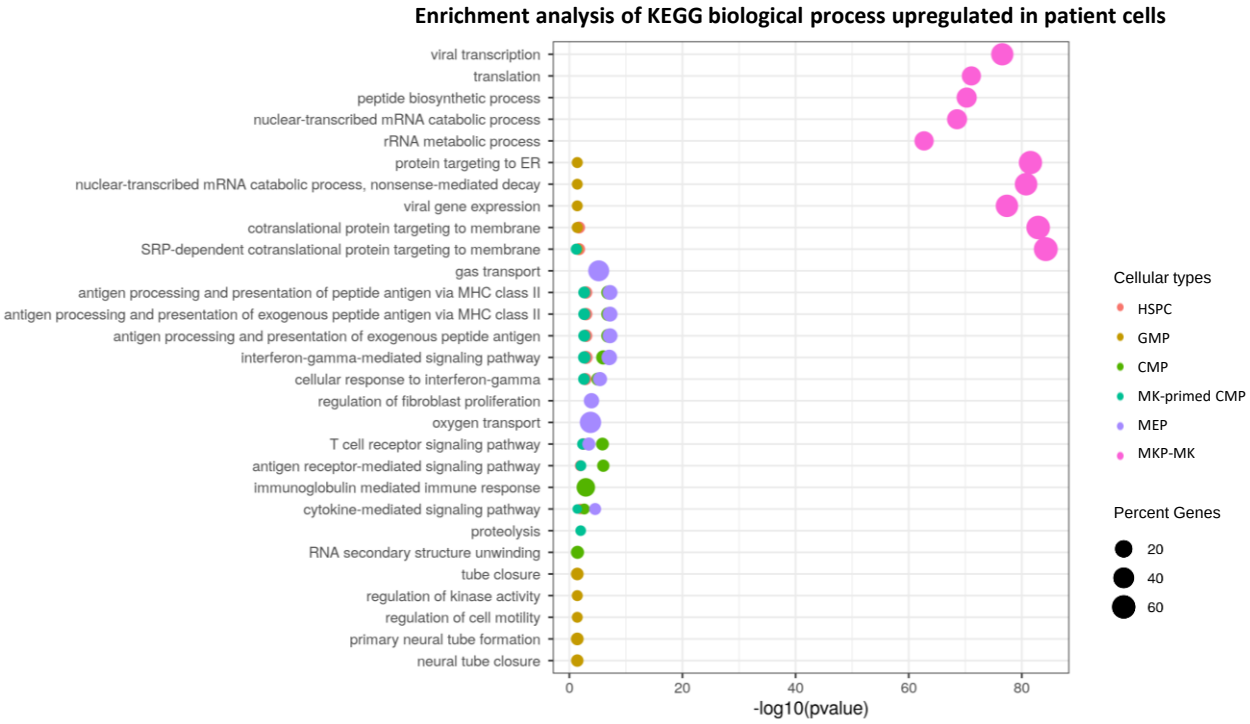

Figure S6: Bubble plot depicting the top upregulated enriched KEGG biological pathways based on differentially expressed genes by cell type. KEGG biological pathways are classified by p-values. Dot sizes reflect the ratio of genes enriched in this pathway to the total number of genes in the pathway. Bubbles are color-coded according to cell type (HSPC, CMP, MK-primed CMP, GMP, MEP, and MKP/MK).

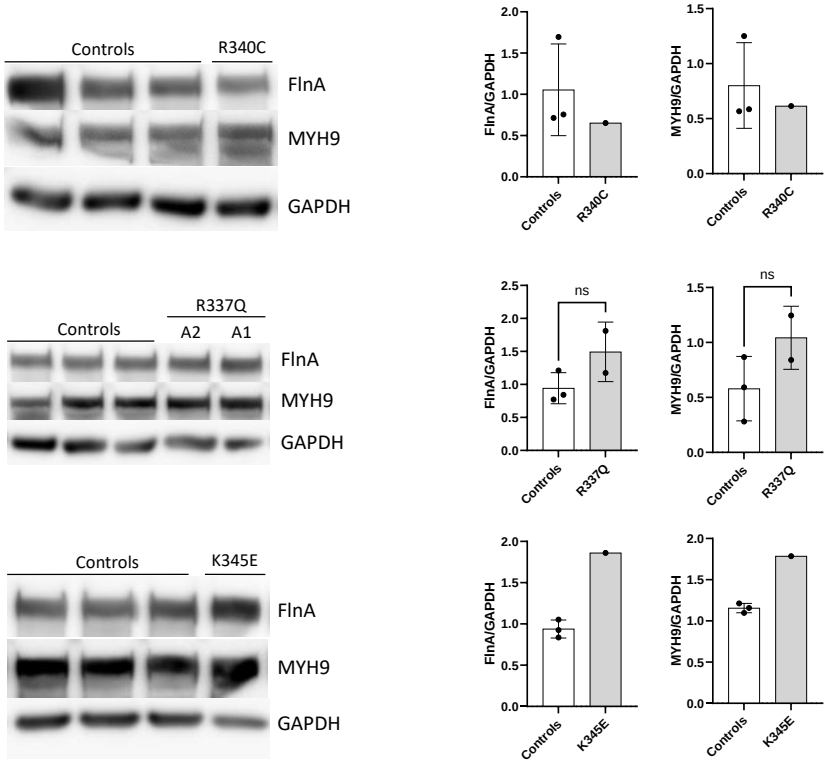

Figure S7: Western blot analysis of FlnA and MYH9 expression in washed platelets from controls and FLI1-variant carriers. GAPDH was used as a protein loading control. Each patient was compared with age- and sex-matched control subjects. For each patient and matched controls, blood samples were collected at the same time and processed in parallel to avoid any bias. Quantification of band intensity is shown on the right.

A

HEL cells

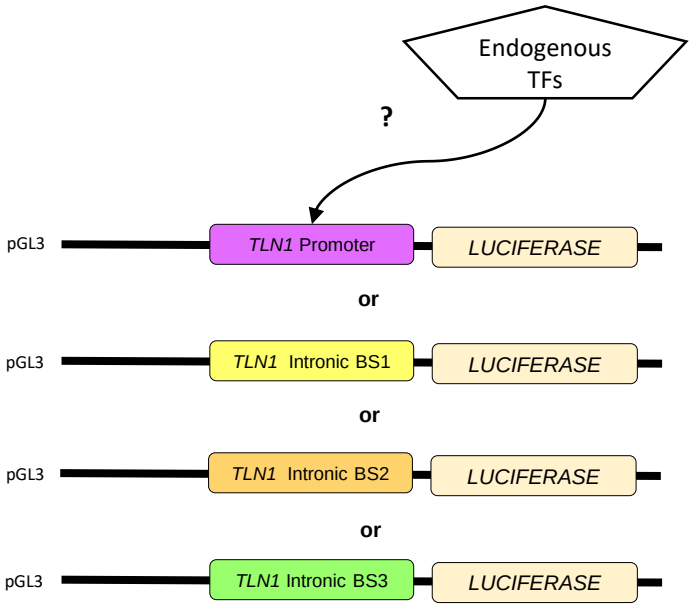

B

MSR cells

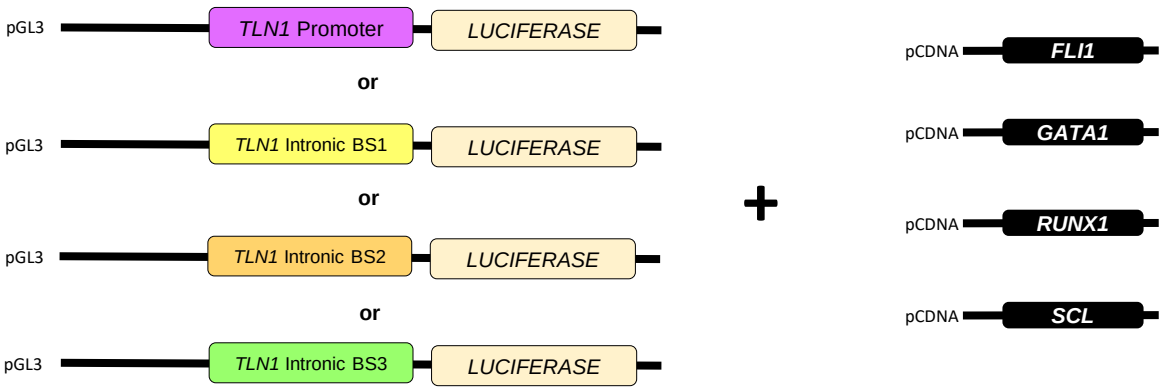

Figure S8: Experimental design of the luciferase reporter assays. Luciferase assays were performed in HEL (A) and MSR (B) cells. Co-transfections of pGL3 reporter vectors with pCDNA vectors were performed according to the ChIP-seq results. TFs: transcription factors; BS: binding site.

A

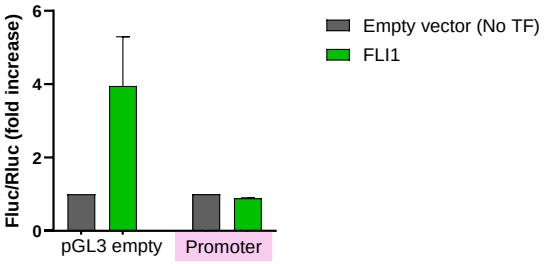

B

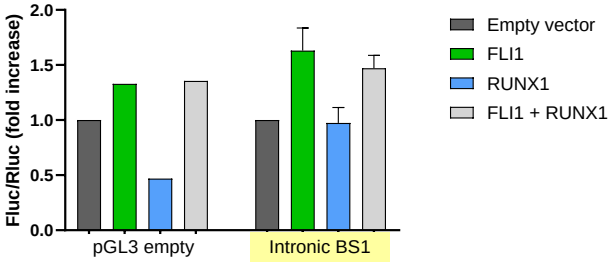

C

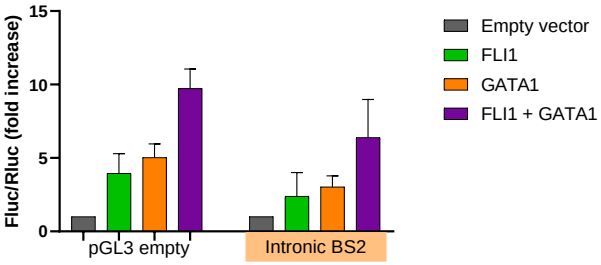

Figure S9: Test of the functionality of *TLN1* regions bound by FLI1. Luciferase reporter assays were performed in MSR cells transfected with DNA sequences corresponding to the promoter (A), intronic binding site 1 (B), and intronic binding site 2 (C) of *TLN1,* along with transcription factors that have binding sites in these sequences based on ChIP-seq analysis. TF: transcription factor; BS: binding site.

SUPPLEMENTARY TABLES

Table S1: Platelet phenotyping in patient C carrying the FLI1 variant R340C.

	Platelet count (x10^9/l)	MPV (fl)	Platelet aggregation maximal intensity (%)			ADP (nmol/10^8 plt)	ATP (nmol/10^8 plt)	ATP/ADP	PRP serotonin levels (µg/10^9 plt)	Mepacrine uptake (MFI)	CD63 (MFI) TRAP6 50 µM
			ADP	Coll*	AA*						
Reference ranges[§]	150-400	8-12	2 µM : 78-95 5 µM : 76-95	85-96	86-96	1.7-3.7	3.5-5.9	1.2-2.4	0.3-1.2	1 µM : 0.66-0.85 2 µM : 0.81-1	1.3-4.23
Patient C	222	11.2	2 µM : 35 5 µM : 60	64	90	0.9	4	4.45	0.15	1 µM : 0.38 2 µM : 0.49	0.93-1.02

MPV: mean platelet volume (measured by optical method using ADVIA, 120, Siemens). [§]The reference ranges were defined as the [minimum-maximum] interval of values obtained from healthy individuals in our laboratory in Marseille. *The collagen and arachidonic acid aggregation assays were performed using agonist concentrations of 2 µg/mL and 0.3 mg/mL, respectively. PLT: platelet; PRP: platelet-rich plasma; ADP: adenosine diphosphate; Coll: collagen; AA: arachidonic acid; ATP: adenosine triphosphate; TRAP: thrombin receptor-activating peptide.

Table S2: Platelet phenotyping in patient D carrying the FLI1 variant G307R.

	Platelet count (x10^9/l)	MPV (fl)	Platelet aggregation maximal intensity (%)			ADP (nmol/10^8 plt)	ATP (nmol/10^8 plt)	ATP/ADP	PRP serotonin levels (µg/10^9 plt)
			ADP	Coll	AA**				
Reference Ranges[¤]	150-400	8-12	2 µM : >28 10 µM : >59	1.25 µg/ml : > 75 5 µg/ml : > 78	> 74	1.7-3.7	3,5-5.9	1.2-2.4	0.3-1.2
Patient D	83-147	13.3	2 µM : 65 10 µM : 85	1.25 µg/ml : 75 5 µg/ml : 81	70	NA	0	-	0.087

**The arachidonic acid aggregation assay was performed using 1 mM AA. [¤]The reference ranges were obtained from healthy individuals at the CHU de Lille, where the patient carrying the G307R variant was characterized. NA: not available.

Table S3: Impact of FLI1 variations on FLI1 DNA-binding domain/DNA interface.

Variation	ΔΔG (kcal/mol)	Type	Effect
G307R	-0.09	Stabilizing	Non-disruptive
R337Q	0.98	Destabilizing	Non-disruptive
R340C	1.49	Destabilizing	Disruptive
K345E	1.48	Destabilizing	Disruptive

Table S4: Impact of FLI1 variations on FLI1 homodimerization.

Variation (FLI1/FLI1)	Interface?	ΔΔG (kcal/mol)	Deleterious?
G307R/G307R	Yes	3.59	Yes
R337Q/R337Q	No	0.27	No
R340C/R340C	No	0.21	No
K345E/K345E	No	0.16	No